REVIEWS

Journal of Semiconductors
(2020) 41, 011201
doi: 10.1088/1674-4926/41/1/011201

Progress on the controllable synthesis of all-inorganic halide perovskite nanocrystals and their optoelectronic applications

Yi Yuan and Aiwei Tang†

Key Laboratory of Luminescence and Optical Information, Ministry of Education, School of Science, Beijing Jiaotong University, Beijing 100044, China

Abstract: In the past five years, all-inorganic metal halide perovskite ($CsPbX_3$, X = Cl, Br, I) nanocrystals have been intensely studied due to their outstanding optical properties and facile synthesis, which endow them with potential optoelectronic applications. In order to optimize their physical and chemical properties, different strategies have been developed to realize the controllable synthesis of $CsPbX_3$ nanocrystals. In this short review, we firstly present a comprehensive and detailed summary of existed synthesis strategies of $CsPbX_3$ nanocrystals and their analogues. Then, we introduce the regulations of several reaction parameters and their effects on the morphologies of $CsPbX_3$ nanocrystals. At the same time, we provide stability improvement methods and representative applications. Finally, we propose the current challenges and future perspectives of the promising materials.

Key words: metal halide perovskite; nanocrystals; synthesis; optical properties

Citation: Y Yuan and A W Tang, Progress on the controllable synthesis of all-inorganic halide perovskite nanocrystals and their optoelectronic applications[J]. *J. Semicond.*, 2020, 41(1), 011201. http://doi.org/10.1088/1674-4926/41/1/011201

1. Introduction

Colloidal semiconductor nanocrystals (NCs), also known as colloidal quantum dots, have inspired intensive study for decades due to their unique optical and electrical properties, which are closely related to their size, dimension and morphology[1–4]. These outstanding properties, such as narrow emission bandwidth, size-dependent emission and high luminescent efficiency, combined with solution-processed ability, contribute to their huge potentials for applications in various optoelectronic devices[5–8]. The past decade has witnessed the impressive development of an ancient but novel type of materials, metal halide perovskite NCs[9–11]. Generally, named after Russian mineralogist Lev Perovski, perovskites refer to a large family of materials adopting a similar crystal structure to calcium titanate ($CaTiO_3$) with a chemical formula of ABX_3. As for the halide perovskite NCs, "A" usually represents methylammonium (MA), formamidinium (FA), cesium (Cs), rubidium (Rb) or the mixture; "B" can be lead (Pb), tin (Sn), bismuth (Bi) or the mixture; "X" refers to halide anions including chlorine (Cl), bromine (Br), iodine (I) or the mixture. The halide perovskite NCs can be divided into hybrid organic–inorganic perovskite NCs, where A is an organic group, and all-inorganic NCs when A is an inorganic cation. Since the first application of $CH_3NH_3PbX_3$ NCs as sensitizers for dye-sensitized solar cells in 2009[12], enormous attention has been attracted to make further exploration into this field[13–15]. Currently, with dramatically fast development speed, the highest power conversion efficiencies (PCEs) of solar cells based on hybrid perovskite NCs has already reached 23%[16], mainly benefiting from their high light absorption coefficients ($> 1 \times 10^4$ cm^{-1}) and long balanced charge-carrier diffusion lengths (> 100 nm). Endowed with outstanding optical properties, the hybrid perovskite NCs are also regarded as promising cost-effective materials for light-emitting diodes (LEDs) and other optical devices[17–19]. However, the hybrid perovskite NCs are extremely sensitive to oxygen, moisture, heat and light due to the existence of organic groups in the structure[20]. In contrast, the all-inorganic perovskite NCs counterparts are ideal candidates as inherently equipped with higher thermal decomposition temperature and more stable crystal structures[21, 22].

In order to efficiently adjust the optical properties of perovskite NCs, it is crucial to understand the relationships between structures and characteristics. As is well known, the metal halide perovskites have three main crystalline structures including cubic, orthorhombic, and tetragonal phases. In these different phases, it is generally believed that the cubic phase appears at relatively high temperature[23], but $CsPbX_3$ NCs can exhibit the cubic phase above room temperature due to size reduction[24]. Commonly, the $CsPbCl_3$ and $CsPbBr_3$ NCs are proven to be relatively stable in composition while the unstable cubic $CsPbI_3$ NCs enjoy the large bandgap for photovoltaic applications (E_g = 1.73 eV)[25]. Taking the crystal structure of cubic $CsPbBr_3$ as an example, as is shown in Fig. 1(a), Cs ions occupy the vertexes of cubes while six Br ions assemble an octahedron with a Pb ion in the center of the framework. Previous reports demonstrate that Cs ions have little effect on the electronic structure of band edge, thus the excitation and recombination of electrons and holes are confined within the $[PbBr_6]^{4-}$ octahedra[24].

Since the first synthesis of colloidal $CsPbX_3$ NCs was reported by Kovalenko and co-workers in 2015[26], tremendous attention has been paid to developing different synthetic strategies for preparing high-quality of colloidal $CsPbX_3$ NCs[24, 27–30]. These studies not only shed light on the growth

Correspondence to: A W Tang, awtang@bjtu.edu.cn
Received 27 SEPTEMBER 2019; Revised 18 NOVEMBER 2019.

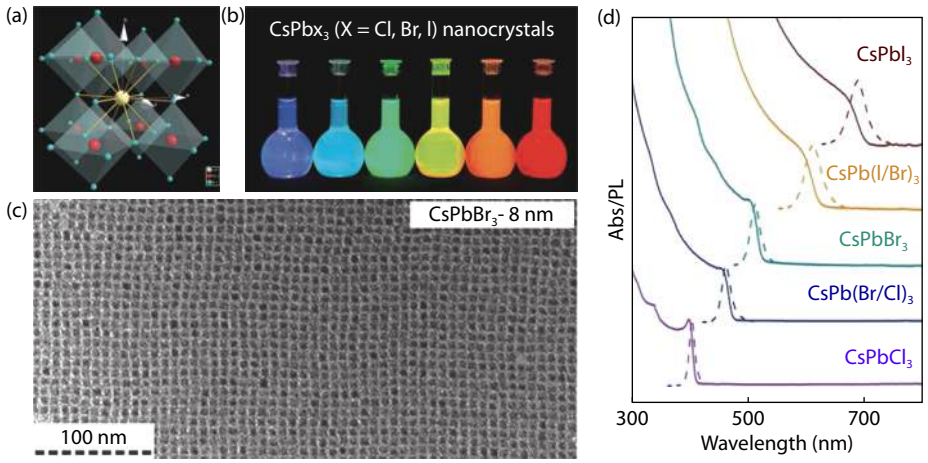

Fig. 1. (Color online) (a) The crystal structure of cubic $CsPbX_3$ NCs. Reproduced with permission from Ref. [24]. (b) Images of $CsPbX_3$ NCs dispersions with different emission colors under the UV light. Reproduced with permission from Ref. [26]. (c) The TEM image of $CsPbBr_3$ NCs with the cubic morphology. Reproduced with permission from Ref. [26]. (d) Absorption and PL spectra of $CsPbX_3$ NCs with different compositions. Reproduced with permission from Ref. [26].

mechanism but also lay a concrete foundation for further practical applications of $CsPbX_3$ NCs. In this work, we will thoroughly review the existing protocols for the controllable synthesis of $CsPbX_3$ NCs and their various analogues by focusing on several key parameters in the reaction process. Besides, strategies for stability improvement will also be generally summarized. At last, a brief introduction to several promising applications of $CsPbX_3$ NCs in sundry fields is presented, with some current challenges and future development perspectives being proposed.

2. Solution synthesis approaches of $CsPbX_3$ NCs

2.1. High temperature synthesis

The first synthesis of all-inorganic metal halide perovskite crystals $CsPbX_3$ (X = Cl, Br or I), and their analogue Cs_4PbX_6 (X = Cl or Br) in solution phase was reported as early as 1893 by Wells and his collaborators[31]. The systematic studies in the structural and physical properties of all-inorganic metal halide perovskites can be traced back to more than sixty years ago, in which Moller studied the crystal structure and photoconductivity of $CsPbX_3$ bulk materials[32]. However, the research failed to attract intensive attention due to the poor optical properties and complex fabrication strategy until the more facile and scalable method to synthesize $CsPbX_3$ NCs was reported by Protesescu and co-workers in 2015[26]. In this work, the colloidal $CsPbX_3$ NCs with uniform cubic shape and outstanding optical properties were successfully synthesized through a hot-injection method. In a typical synthesis, specific amount of Pb(II) halide (PbX_2) powder is dissolved into a degassed mixture of the surfactants (usually organic amine and organic acid, OAm and OA) and the solvent (usually octadecene), followed by quick-injection of the heated pre-synthesized Cs precursor (usually Cs-oleate) into the reactant at a certain temperature (usually 120–200 °C). The very fast nucleation and growth of the $CsPbX_3$ NCs can finish within several seconds owing to the intrinsic ionic crystal feature. Consequently, the size of cubic $CsPbX_3$ NCs can be tuned effectively by changing the reaction temperature or the precursor concentration rather than the growth time. The schematic diagram of the hot-injection method is presented in Fig. 2(a). The all-inorganic perovskite NCs with mixed halide composition, such as $CsPb(Cl/Br)_3$ and $CsPb(Br/I)_3$, can be easily achieved through changing the ratios of PbX_2 ingredients. Figs. 1(b)–1(d) show the uniform cubic shape and outstanding optical properties of the as-synthesized $CsPbX_3$ NCs. The facile and efficient hot-injection method of $CsPbX_3$ NCs lays a concrete foundation for the following intensive study of the unique properties and wide applications.

In 2017, Yerama *et al.* applied an under the pressure-assisted hot-injection approach to realize a linearly upscale synthesis of $CsPbBr_3$ NCs[33]. In a typical synthesis, the reactor is maintained vacuum to heat the PbX_2 precursor, followed by the injection of warm Cs-oleate under a mild vacuum with the pressure reaching 1−10 mbar. The under pressure-governed hot-injection method could yield multigram-scale $CsPbBr_3$ NCs, 200 times more compared with the traditional method, with a narrow emission width (~22 nm) and a high photoluminescence quantum yield (PLQY) of 76%.

In addition, Chen *et al.*[34] reported a one-pot strategy based on the conventional synthesis method, in which all reagents, including PbX_2 (X = Cl, Br, and I) salts solution and Cs-oleate solution, were loaded into a single reaction pot and subsequently heated to the desired reaction temperature in air. The as-synthesized $CsPbX_3$ exhibited a shape of quantum dots instead of nanocubes. This non-injection method can yield a large amount of high-quality NCs on the gram scale with a one-batch reaction. It also can realize size control, compositional modulation and band-gap tuning simultaneously, which pave the way for further applications.

2.2. Room temperature synthesis

Although the hot-injection method conducted at high temperatures has been widely applied, several problems still remain to be solved. For example, the scalable synthesis may not be achievable using this hot-injection method due to the requirement of conventional heating, inert atmosphere and injection conditions. Besides, the modification scope of morphology and optical properties is very limited at high temperatures. To compensate for the disadvantages of the hot-injection method, partially inspired by a ligand-assisted re-crystallization strategy to fabricate hybrid $CH_3NH_3PbX_3$ NCs[35],

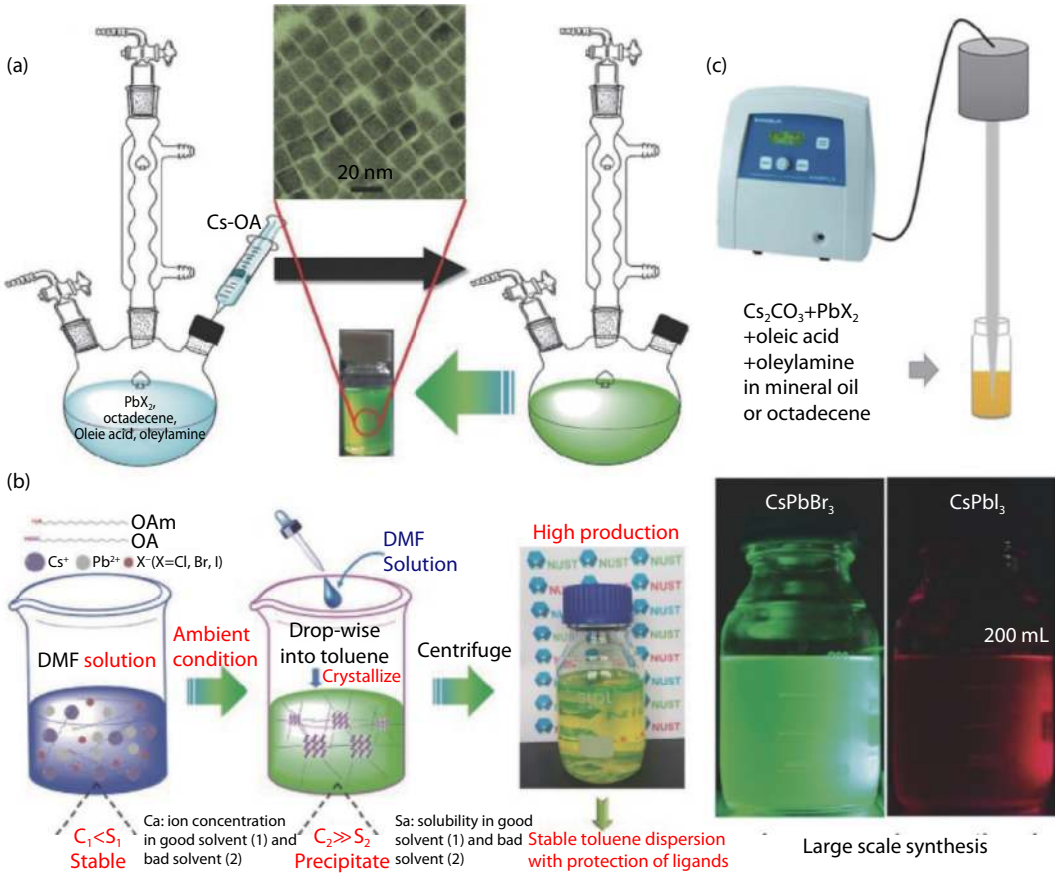

Fig. 2. (Color online) (a) Schematic of the hot-injection method. The digital graph and TEM image of the corresponding sample are shown as insets. Reproduced with permission from Ref. [24]. (b) Schematic of the room temperature fabrication strategy. The digital graph of as prepared $CsPbBr_3$ NCs dispersion is presented aside. Reproduced with permission from Ref. [24]. (c) Schematic of the single-step tip ultrasonication synthesis. The digital images of as-prepared $CsPbBr_3$ and $CdsPbI_3$ NCs are shown as below. Reproduced with permission from Ref. [37].

Zeng group developed a complementary re-crystallization method through creating a supersaturated condition when inorganic ions including Cs^+, Pb^{2+} and X^- transformed from good solvents into poor solvents at room temperature[36]. The schematic illustration of the synthesis route is shown in Fig. 2(b). Firstly, CsX and PbX_2 (X = Cl, Br, I or their mixtures) of specific amounts under their solubility are dissolved completely in a good solvent (dimethyl formamide (DMF) or dimethyl sulfoxide (DMSO) commonly), with surfactants (OAm and OA). Subsequently, a small amount of the above solution is added into a bad solvent (usually toluene). The solubility of inorganic ions in toluene is much smaller (within 10^{-7} g/mL) while DMF or DMSO and toluene are mutually soluble. Given that metal ions are insoluble in toluene (within 10^{-7} g/mL), a highly supersaturated state is produced immediately inducing a rapid re-crystallization of $CsPbX_3$ NCs in the mutually mixed solution. In this case, surfactants can help to disperse all precursors in various nonpolar solvents and to control the size, shape and optical properties as well. Apart from the re-crystallization method, ultrasonication is another method for synthesis of $CsPbX_3$ NCs at room temperature. Tong *et al.*[37] developed a versatile, polar-solvent-free and single-step approach for scalable synthesis of highly luminescent $CsPbX_3$ NCs with tunable-thickness through ultrasonication. As shown in Fig. 2(c), the precursors consisting of Cs_2CO_3, PbX_2 and surface ligands (OAm and OA) are dissolved in a nonpolar solvent (mineral oil or octadecene). The sonication firstly induces the formation of the Cs-oleate and then helps to yield the colloidal $CsPbX_3$ NCs, which exhibit enhanced air stability. Although the $CsPbX_3$ NCs are obtained at room temperature without inert atmosphere protection, they still exhibit comparable optical properties to that of NCs synthesized at high temperatures using hot-injection method.

2.3. Template-assisted synthesis

Traditional colloidal $CsPbX_3$ NCs with organic ligands capped on the surface are easily aggregated, resulting from the strong dispersive interactions of the surfactants[38]. Moreover, for the tiny $CsPbX_3$ NCs, there are usually difficulties in the isolation and purification process[39]. To solve this problem, Kovalenko *et al.* reported another facile, non-colloidal and ligand-free strategy to prepare a large variety of perovskite $APbX_3$ NCs using mesoporous silica (meso-SiO_2) as a growth template[40] (Fig. 3(a)). This method benefits a lot from the unique defect-tolerant character of perovskite NCs, getting rid of the strict demanding of surface-passivation[9]. In the synthesis, various commercially available mesoporous silica templates (preheated to 50 °C) are firstly immersed into highly concentrated solutions of the precursor salts (AX and PbX_2), which exceeds the pore volume of the template. Then, the mixture is stirred in an inert atmosphere at room temperature to achieve the full impregnation. Afterwards, excess solution is removed through filtration to prevent the formation of perovskite crystals outside the pores. Finally, the as-obtained samples are dried under vacuum at a relatively high temperature. The as-prepared perovskite NCs exhibit pretty

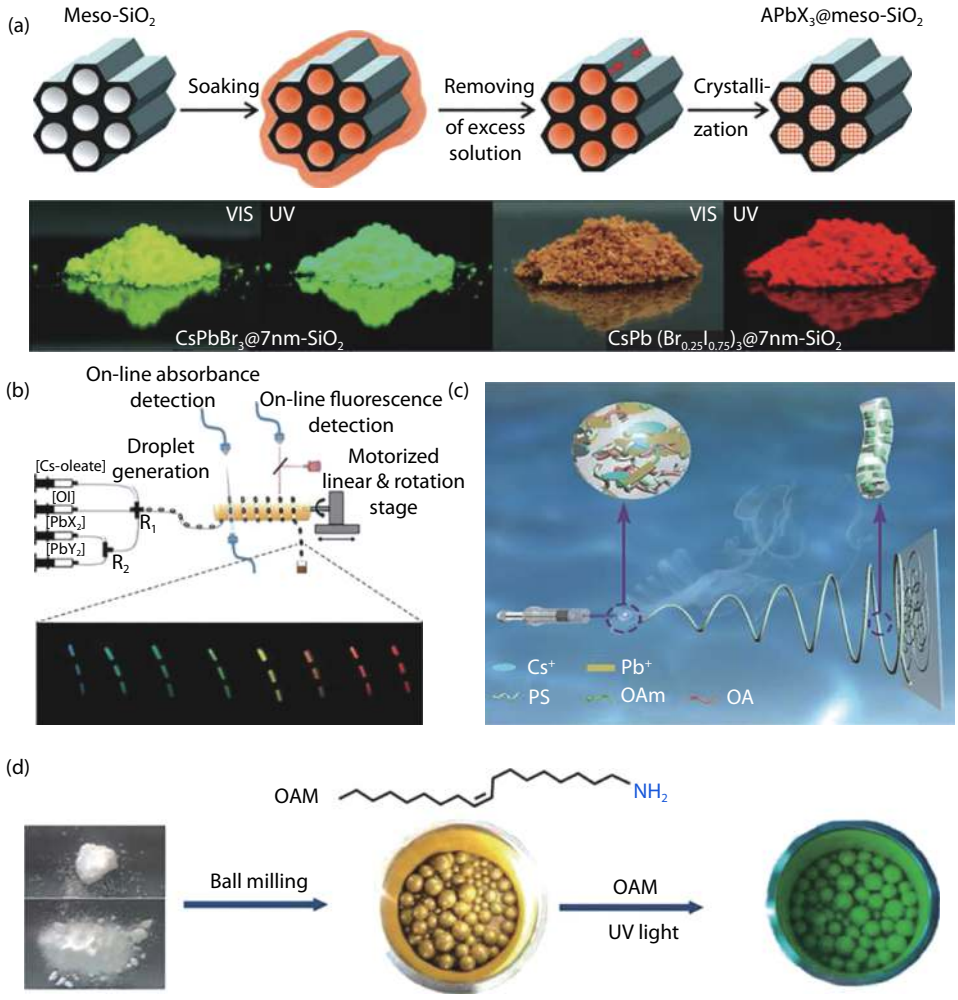

Fig. 3. (Color online) (a) Flowchart of the template-assisted synthesis of $CsPbX_3$ NCs in the pores of mesoporous silica, and photographs of mesoporous silica impregnated with $CsPbBr_3$ (left) and $CsPb(Br_{0.25}I_{0.75})_3$ NCs (right) under daylight and under UV illumination. Reproduced with permission from Ref. [40]. (b) Illustration of the droplet-based microfluidic platform integrated with online absorbance and fluorescence detection for the synthesis and real time characterization of $CsPbX_3$ NCs. Reproduced with permission from Ref. [43]. (c) Illustration of *in-situ* growth of all-inorganic $CsPbX_3$ nanocrystals in the polymers via one-step electrospinning technique. Reproduced with permission from Ref. [44]. (d) Schematic and photographs of mechano-synthesis of $CsPbX_3$ NCs and their fluorescence under UV light irradiation during ball milling. Reproduced with permission from Ref. [45].

high PLQY exceeding 50%. Furthermore, as the size of the NCs can be controlled facilely by choosing different silica templates, such as hexagonally ordered one-dimensional channels (2.5–7 nm pore widths), interconnected cubically ordered cavities (3 nm), or disordered pore networks (15–50 nm pore widths) of a specific characteristic size, this protocol can also open the possibility of a systematic way to study the size-dependent properties at small sizes.

2.4. Microwave synthesis

The simple, efficient and microwave-assisted protocol was developed by the Zhang group[41], and different-shaped colloidal $CsPbX_3$ NCs are successfully synthesized, which exhibit and the highest PLQY of 75%. During the synthesis process, all precursors, including cesium acetate (CsOAc), lead halide, trioctylphosphine oxide (TOPO), OA, OAm, and octadecene (ODE), are simply mixed in a microwave quartz tube without any pre-synthesis of Cs-oleate. By simple microwave irradiation, stable colloidal $CsPbX_3$ NCs in the shapes of nanocubes, nanorods, NWs, quadrate nanoplates and hexagonal nanoplates can be achieved.

2.5. Droplet-based synthesis

Microfluidic reaction systems have been widely used in the mechanism study or the fine-tuning of reaction factors[42]. As far as the formation mechanism of $CsPbX_3$ NCs is concerned, the accurate and systematic understanding of related parameters is very limited because of the extremely fast kinetics and intricate involved variables[26]. Consequently, Kovalenko and coworkers adopted a droplet-based microfluidic platform to *in-situ* gain the insights into the formation of $CsPbX_3$ NCs over a millisecond to several seconds time span[43]. Meanwhile, the online photoluminescence and absorption measurements allow the rapid depiction of various governing factors, such as the molar ratios of precursors, compositions and temperatures (Fig. 3(b)).

2.6. Electrospinning synthesis

Very recently, Liao and co-workers reported a general one-step electrospinning strategy for *in-situ* growth of all-inorganic perovskite NCs in polymer fibers (Fig. 3(c))[44]. The optical properties of the as-prepared perovskite NCs@polymer fibers

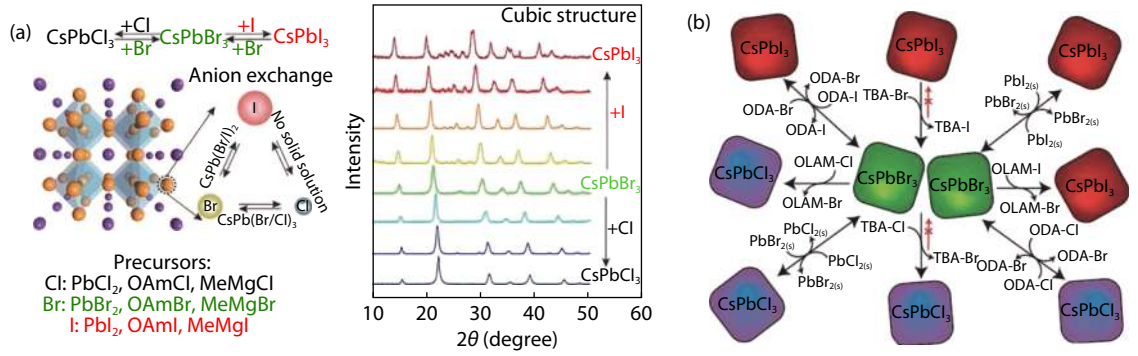

Fig. 4. (Color online) Overview of the different anion-exchange routes and precursors within the cubic $CsPbX_3$ NCs and their corresponding XRD patterns reported by (a) Kovalenko group and (b) Manna group respectively. Reproduced with permission from Refs. [49, 50].

can be readily tuned by tailoring the compositions of lead halide and cesium halide precursors within the electrospinning solution, allowing their PL emission covering the whole visible range. What's more, the stability against water and thermal of the composites was fundamentally enhanced, with their PLQYs keeping 70% of its original value after immersion in water for 192 h and maintaining over 50% at 80 °C for 2 h.

2.7. Non-solvent synthesis

Currently, the most synthesis methods of $CsPbX_3$ NCs fail to avoid using toxic solvents. In order to realize the environmental-friendly production of $CsPbX_3$ NCs, Zhu *et al.* developed a new mechano-synthesis strategy which is free of solvent and high reaction temperature[45]. The simplified synthesis process is depicted in Fig. 3(d). Taking the synthesis of $CsPbBr_3$ NCs as an example, the metal salts CsBr and $PbBr_2$ are directly mixed through high-speed mechanically milling or grinding. The color of the precursors would change into yellow and $CsPbBr_3$ NCs or partial bulk products appeared within a few minutes. Subsequently, further surface treatment with OAm was necessary to improve the luminescence of the $CsPbBr_3$ NCs[46]. The rationale may be attributed to the reactivity of the mobile phase on the exposed solid reactants' surfaces[47]. This mechano-synthesis method provides the greenest avenue in the preparation $CsPbX_3$ NCs.

Non-solvent preparation of $CsPbX_3$ NCs can be realized through the gas-phase synthesis as well. For instance, Jin group[48] explored a facile and general chemical vapor deposition (CVD) method to fabricate $CsPbX_3$ nanowires (NWs) and microwires (MWs), in which a mixture of CsX and PbX_2 powders as precursors heated in the middle of the furnace at about 300 to 350 °C in the flow of argon gas. The as-prepared $CsPbX_3$ NCs were horizontally oriented with high density in mica, and a variety of $CsPbBr_3$ nanostructures, including Y-shaped branches or interconnected NW or MW networks can be achieved via simple tuning the deposition time. The as-synthesized high-quality ligand-free $CsPbX_3$ networks grown on mica substrates could serve as outstanding substrates for photoelectronic devices and other applications.

2.8. Anion exchange reaction

The optical properties can be conveniently controlled by tuning the halide compositions of the precursors during the synthesis of $CsPbX_3$ NCs. However, the synthesis of highly bright pure $CsPbCl_3$ NCs and $CsPbI_3$ NCs is usually not as easy as that of $CsPbBr_3$ NCs. Fortunately, similar to their organic-inorganic hybrid counterparts, a more facile post-synthetic compositional modulation method was developed by Kovalenko group[49] and Manna group[50] independently almost at the same time. Thanks to their ionic features, the bandgap and PL emission are readily tunable over the entire visible spectral region through the fast halide anion-exchange reaction. $CsPbBr_3$ NCs are commonly chosen as the initial materials due to their good stability and strong fluorescence. Several types of halide sources have been investigated, which include the simple PbX_2 salts, organometallic Grignard reagents (MeMgX), oleylammonium halides (OAmX), octadecylammonium halides (ODAX), tetrabutylammonium halides (TBAX). The anion-exchange reaction quickly happens within seconds upon the mix of $CsPbBr_3$ NCs and halide precursors together, leading to a blue shift (Br to Cl or I to Br routes) or a redshift (Br to I or Cl to Br routes) of the PL emission wavelength. Besides, it is worth to be noted that this anion exchange reaction can occur by directly mixing $CsPbX_3$ NCs of different halide compositions as well, even without any additional halide sources. The shape, crystal structure and even the PL properties of the as-obtained NCs are almost identical to their parent NCs, except a little size change after the anion-exchange. As is mentioned above, the synthesis of $CsPb(Cl/I)_3$ NCs is not available due to the significant difference in the ionic radii. Accordingly, the anion-exchange works only for the Cl–Br and Br–I couples in both directions, but never from $CsPbCl_3$ to $CsPbI_3$ nor in the reverse direction. Treating $CsPbCl_3$ NCs with a large excess of iodide source would give rise to transforming the PL color from blue directly to red, lacking any intermediate colors, and vice versa. Fig. 4 shows the overview of different routes and precursors for the anion-exchange reactions on $CsPbX_3$.

3. Analogues of $CsPbX_3$ NCs

In a broad sense, the general formula of the all-inorganic cesium lead halide perovskites can be written as $Cs_aPb_bX_{a+2b}$, where the most common structure is $CsPbX_3$ ($a = 1$, $b = 1$). Although the elemental compositions of these analogues are similar, their crystal structures are totally different. For the $CsPbX_3$ NCs, as is mentioned above, the $[PbX_6]^{4-}$ octahedrons are corner-shared in the unit cells (Fig. 1(a)), which is considered as a three-dimensional (3D) structure. As regards the $CsPb_2X_5$ NCs and Cs_2PbX_4 NCs, both named two-dimensional (2D) structures, the $[PbX_6]^{4-}$ octahedrons tend to form planes with Cs^+ inserted between them. The $[PbX_6]^{4-}$ octahedrons in the Cs_4PbX_6 NCs are separated from each other while Cs^+ cations

fill the centers of four adjacent $[PbX_6]^{4-}$ octahedrons, forming the zero-dimensional (0D) structure consequently.

Some reports have demonstrated remarkable improvement in the optical properties of perovskite materials with a reduction of dimensionality[51–53]. As for the 2D structures, the $CsPb_2Br_5$ nanoplates obtained by the precipitation reaction and fast anion exchange was reported by Yu group[54], whose PLQY in solution was claimed to reach 87% and PL spectra were able to cover the entire visible spectral region. Besides, the $CsPb_2X_5$ NWs were also successfully prepared by Deng group through a ligand-mediated method with enhanced stability[55]. In addition, a dual-phase composite $CsPbBr_3$-$CsPb_2Br_5$ NCs were synthesized by Sun group[56]. The parasite of $CsPb_2Br_5$ phase on the cubic $CsPbBr_3$ NCs could reduce diffusion length of excitons and decrease the trap density. The $CsPb_2Br_5$ microplates were also successfully prepared by Tang *et al*.[57]. Besides, very recently, another all-inorganic perovskite analogue enjoying two-dimensional phase was reported for the first time with the hybrid composition of $Cs_2PbI_2Cl_2$[58]. This compound exhibited a direct bandgap of 3.04 eV and a large in-plane resistivity. A strong UV-light response and an effective in-plane α-particle counting ability make this 2D perovskite polymorph a very promising optoelectronic material.

Some work on the 0D Cs_4PbX_6 NCs indicates that the NCs exhibit outstanding luminescent properties as well. For example, novel perovskite-related Cs_4PbBr_6 semiconductors were fabricated by an easy interface reaction strategy in a liquid–liquid immiscible two-phase system[59]. Although the particle sizes were on the micrometer scale, the PLQY could reach 40%–45%. Mohammed and co-workers[60] reported a facile room-temperature synthesis of pure Cs_4PbBr_6 NCs in solid and claimed the high luminescence properties with a 45% PLQY of this 0D perovskite derivative. The exciton binding energy was estimated to be 353 meV.

However, there are still some controversies lying in the accurate luminescence mechanism of these perovskite polymorphs. Some researchers argue that the bright luminescence probably arises from the inevitable presence of highly luminescent $CsPbX_3$ NCs even at quite low concentrations[56, 61]. Meanwhile, recent related studies have firmly confirmed the discontinuous electronic structures and ultra-large bandgap of Cs_4PbX_6 due to its decentralized crystal structure, which is scarcely possible to be highly luminescent[62, 63]. Moreover, the bandgap of $CsPb_2Br_5$ was measured to be 2.98 eV, thus revealing the theoretic weak PL emission[64].

An interesting phenomenon is the easy phase transformation of these perovskite analogues between each other under various conditions, such as the extra addition[62] or extraction[65, 66] of precursors, ligand-mediation[63, 67, 68], light induction[67] and so on. As to the transformation from Cs_4PbX_6 to $CsPbX_3$, the process can be both considered as the addition of PbX_2 or the extraction of CsX, thereby the Cs_4PbX_6 should be regarded as a PbX_2-deficient structure or a CsX-rich structure accordingly. Manna group tried to convert the non-luminescent Cs_4PbX_6 NCs to the luminescent $CsPbX_3$ NCs by adding extra PbX_2 into the pure Cs_4PbX_6 NCs synthesized in a Cs-rich environment[62]. As is shown in Fig. 5(a), the distinctions of optical properties and morphologies after injection of PbX_2 can be clearly observed. However, Zhang group[65] realized this phase transformation from the other perspective via an ingeniously designed experiment. In detail, a two-phase reaction system was established and the non-luminescent Cs_4PbX_6 NCs were dispersed in a nonpolar organic phase while the other phase was dispersed in water. Since the solubility of CsX salts in water was very high, the CsX composition in the Cs_4PbX_6 NCs was quickly stripped across the oil/water interface into the water phase (Fig. 5(b)). Consequently, the highly luminescent $CsPbX_3$ NCs layer gradually formed and expanded with the reaction time prolonging. More importantly, the as-obtained NCs were proved to be more stable than those $CsPbBr_3$ NCs prepared through the traditional hot-injection method, which could be attributed to the possible passivation during the water treatment.

Also by the Manna group[66], the transformation from Cs_4PbX_6 to $CsPbX_3$ through the extraction of CsBr could also be achieved either by thermal annealing (physical approach) or by chemical reaction with Prussian Blue (chemical approach) (Fig. 5(c)). According to their results, the physical approach could be facilely carried out on a dried film without addition of any chemicals, while the reaction with Prussian Blue in solution could generate a full transformation into the $CsPbX_3$ phase.

Surface ligands also play a significant role in the phase tuning. For instance, the Alivisatos group[63] invented a ligand-mediated method for phase transformation from $CsPbBr_3$ NCs to the Cs_4PbBr_6 derivative, which was governed by a two-step dissolution-recrystallization mechanism (Fig. 5(d)). In this process, the OAm was added to trigger the transformation reaction, and alkyl-thiol ligands acted as the modulator to improve the size uniformity and chemical stability of the Cs_4PbBr_6. Similarly, a reversible structural and compositional transformation between cubic $CsPbX_3$ NCs and rhombohedral Cs_4PbX_6 NCs was induced through the precisely controlling the ratio of OAm to OA ligands[69] (Fig. 5(e)). As was revealed by the surface analysis, the ligand shell of $CsPbBr_3$ NCs consisted of bonded ammonium ligands and OA, while the ligand shell of Cs_4PbBr_6 was composed of both OAm and OA both in a bonded state. As a result, the reversible transformation could be tuned via the acid-base equilibrium. In contrast, the study on the transformation between $CsPbX_3$ NCs and $CsPb_2X_5$ NCs is relatively limited. Deng group[70] reported a strategy for using alkyl-thiols to induce the transformation of $CsPbBr_3$ to $CsPb_2Br_5$ with controlled morphology by rational tuning the ratios of the alkyl-thiol ligands to alkyl-amines or to alkyl-acids (Fig. 6(a)). A novel reversible light-mediated compositional and structural transition process from orthorhombic $CsPbBr_3$ to tetragonal $CsPb_2Br_5$ nanosheets or vice versa was demonstrated in their following work (Fig. 6(b))[67].

Pb is known as a highly toxic element which is one of the major barriers to hinder the commercialization of $CsPbX_3$ NCs. To solve this problem, several replacements, such as tin (Sn), manganese (Mn), germanium (Ge), bismuth (Bi) and antimony (Sb), have attracted great attention[68, 71–76]. Cation exchange reaction can be an effective method to introduce these divalent elements[77]. Among these environment-friendly substitutions, $CsSnX_3$ perovskites and their derivatives are regarded as the most promising materials. The lead-free $CsSnX_3$ NCs are very sensitive to moisture and air, because the Sn^{2+} ions are very easy to be oxidized to Sn^{4+}. The

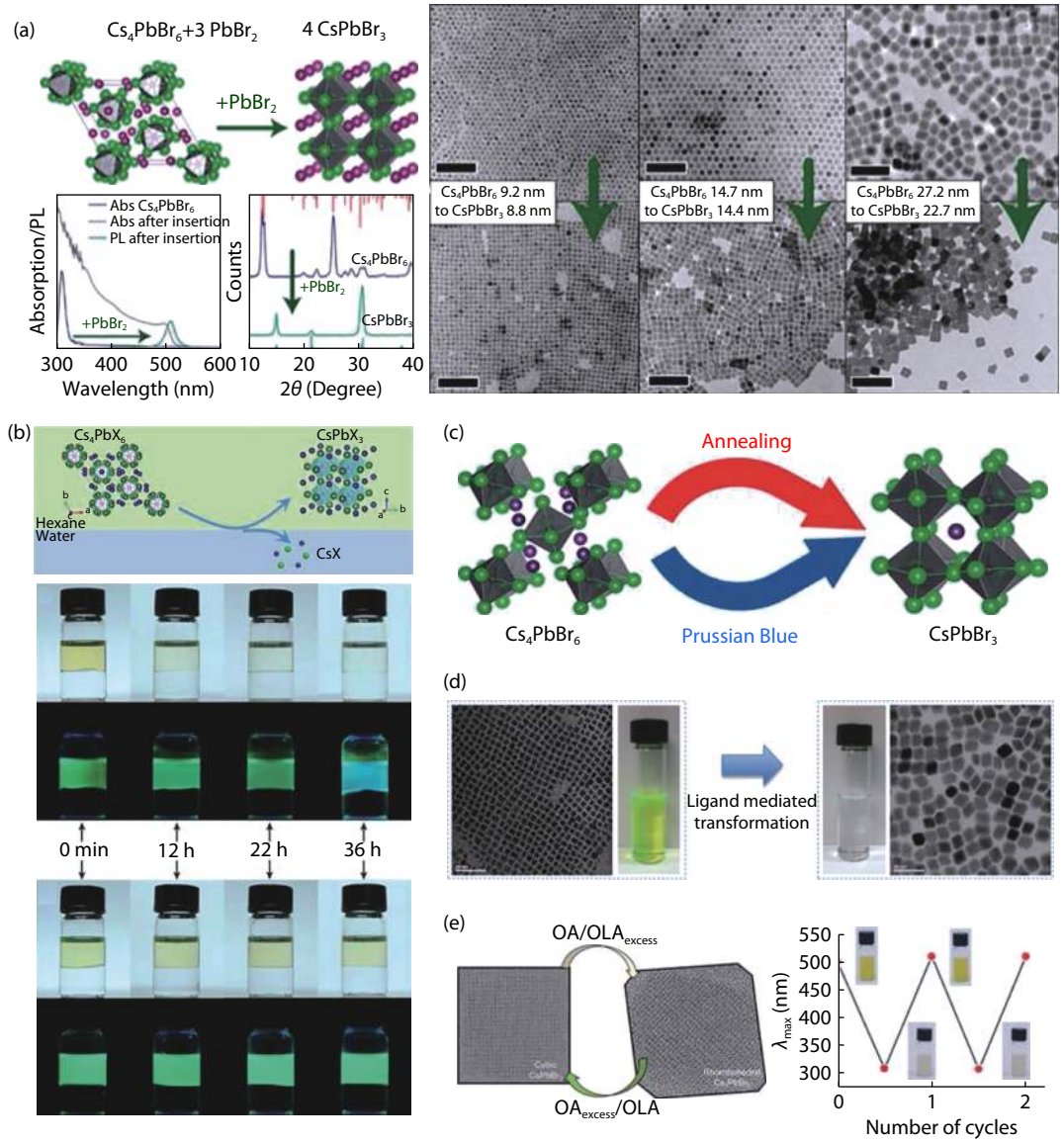

Fig. 5. (Color online) (a) Schematic diagram of the evolution process of Cs_4PbBr_6 to $CsPbBr_3$ NCs with addition of extra $PbBr_2$. Corresponding emission and PL spectra, XRD patterns and TEM images before and after the treatment are shown aside. Reproduced with permission from Ref. [62]. (b) Schematic illustration of of the transformation from Cs_4PbBr_6 to $CsPbBr_3$ NCs with stripping of CsBr. Below are photographs under daylight and UV light, showing the stability of $CsPbBr_3$ NCs obtained through hot-injection method (upper row) and water-triggered transformation process (bottom row). Top layer, $CsPbBr_3$ NCs dispersed in hexane; bottom layer, water. Reproduced with permission from Ref. [65]. (c) Illustration of Cs_4PbBr_6 to $CsPbBr_3$ NCs through the extraction of CsBr achieved either by thermal annealing (physical approach) or by chemical reaction with Prussian Blue (chemical approach). Reproduced with permission from Ref. [66]. (d) Illustration of ligand mediated transformation of pre-synthesized $CsPbBr_3$ to Cs_4PbBr_6 NCs initiated by amine addition. Reproduced with permission from Ref. [63]. (e) Schematic of the ligand control of the dynamic reversibility between $CsPbBr_3$ and Cs_4PbBr_6 NCs. On the left are TEM images of cubic $CsPbBr_3$ to Cs_4PbBr_6 NCs from left to right, and on the right are two complete $CsPbBr_3$ to Cs_4PbBr_6 NCs cycles by ultraviolet–visible spectroscopy. Reproduced with permission from Ref. [69].

Cs_2SnI_6 NCs were successfully synthesized by a modified hot-injection method[78]. Prepared from SnX_4 precursors, Cs_2SnI_6 NCs were found to be more stable under ambient conditions than $CsSnX_3$ NCs, and perhaps potential materials for utilization in solar cells. So far, several strategies have been mainly reported to improve the stability of $CsSnBr_3$ NCs. Firstly, excess fluoric additives, such as SnF_2[79] and perfluorooctanoic acid[80], can effectively suppress the oxidation of Sn^{2+} because the F^- acting as a strong electron-withdrawing group has a stronger interaction with Sn^{2+}. Besides, strong steric hindrance of branched ligands can also prevent the structure of the $CsSnX_3$ NCs from O_2 and H_2O attack[81].

4. Shape control of $CsPbX_3$ NCs

Briefly, various parameters such as reaction temperature, reaction time and surface ligands have significant effects on the shape, size and surface properties of all inorganic halide perovskite NCs, which should be taken into thorough consideration in the controllable synthesis. A series of investigations have been conducted in order to systematically clarify the sundry effects of reaction parameters on the shape control of $CsPbX_3$ NCs.

4.1. Effects of surface ligands

The NCs often have a high specific surface area, and the

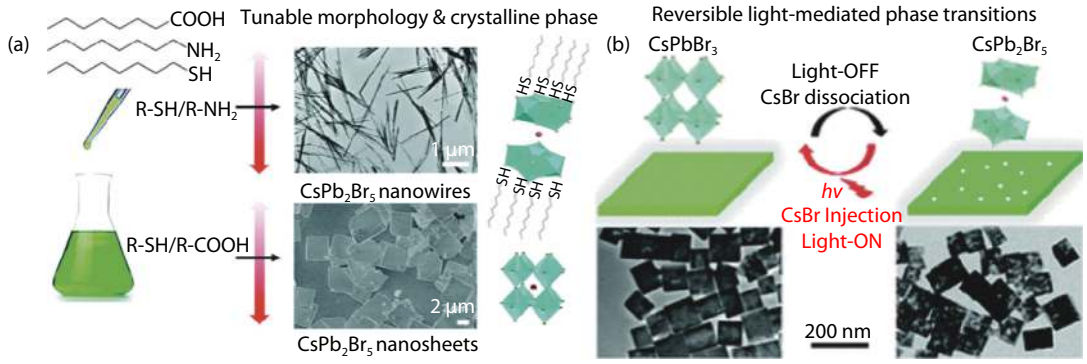

Fig. 6. (Color online) (a) Schematic illustration of the transformation from $CsPbBr_3$ to $CsPb_2Br_5$ NCs induced by alkyl-thiols, with controlled morphologies by tuning the ratios of alkyl-thiols to amines and acids. Reproduced with permission from Ref. [70]. (b) Schematic diagram of reversible light-induced structural transitions from orthorhombic $CsPbBr_3$ to tetragonal $CsPb_2Br_5$ nanosheets. Reproduced with permission from Ref. [67].

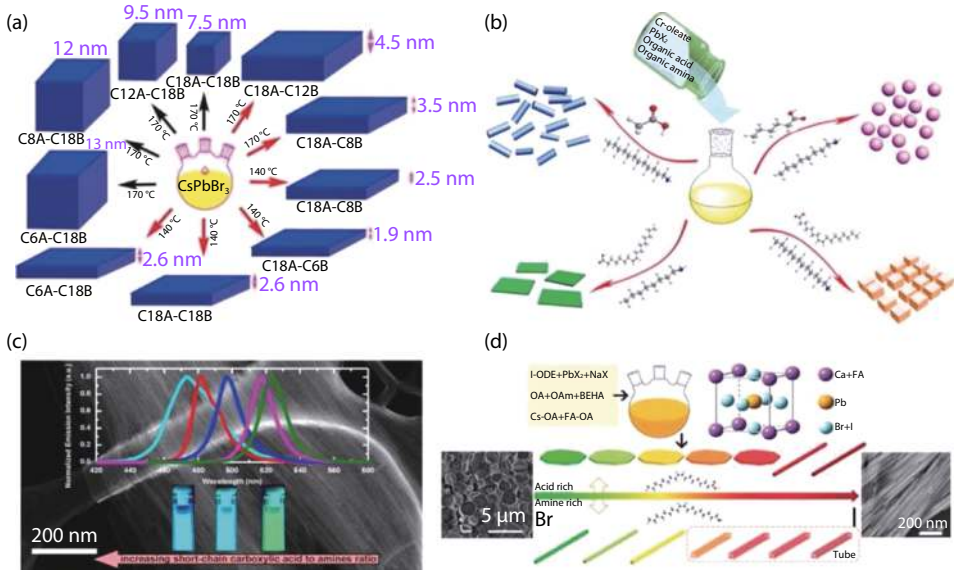

Fig. 7. (Color online) (a) Summary of the shape and size dependence on the chain length of carboxylic acids and amines via hot injection method. Reproduced with permission from Ref. [82]. (b) Overview of $CsPbX_3$ NCs with different morphologies by varying the organic acid and amine ligands at room temperature. Reproduced with permission from Ref. [83]. (c) Illustration of the effect of increasing the ratio of short chain carboxylic acid to amine ligands on controlling the width of the $CsPbBr_3$ NWs. Reproduced with permission from Ref. [84]. (d) Illustration of the morphology control of perovskite NCs tuned by the amount of organic amines and organic acids during the synthesis process. Reproduced with permission from Ref. [86].

surface chemistry can remarkably affect the physical and chemical properties of NCs, which is often used as a fundamentally important modulator in control of their surface modification, shape, luminescent efficiency and stability. For the NCs capped with organic surfactants, the role of amino and carboxylic functional groups is indispensable for the successful controllable synthesis. When it comes to the effects of the organic surface ligands on the shape control or other oriented behavior of the $CsPbX_3$ NCs, the amount and carbon chain length as well as the molecular structure of the organic surfactants are commonly taken into consideration.

To get a thorough understanding of the effects of carbon chain lengths on the shape of the perovskite NCs, Pan *et al.*[82] carried out a comprehensive study to probe the roles of different pairs of carboxylic acids and organic amines with varying chain lengths in the ligand-mediated synthesis of the all-inorganic perovskite NCs. According to their results, as is shown in Fig. 7(a), the organic amines played a more effective role in the shape control of the NCs, leading to the growth of anisotropic platelet structures, while the ammonium ions bound more weakly to the surface than the carboxylate ligands. The morphology of $CsPbBr_3$ NCs tended to become thinner nanoplatelets when shorter chain amines were used, while the larger nanocubes were achieved at high temperature reactions when shorter chain carboxylic acids were involved. This phenomenon probably resulted from the faster diffusion of short amines, leading to the faster exchange rates and anisotropic growth of the $CsPbX_3$ NCs. Additionally, the binding between the organic ligands and the surfaces may be weakened under high temperature, thus giving rise to larger $CsPbX_3$ NCs.

Another systematic study focusing on the ligand-mediated approach to control the shape of $CsPbX_3$ NCs at room temperature was conducted by the Deng group[83]. They pro-

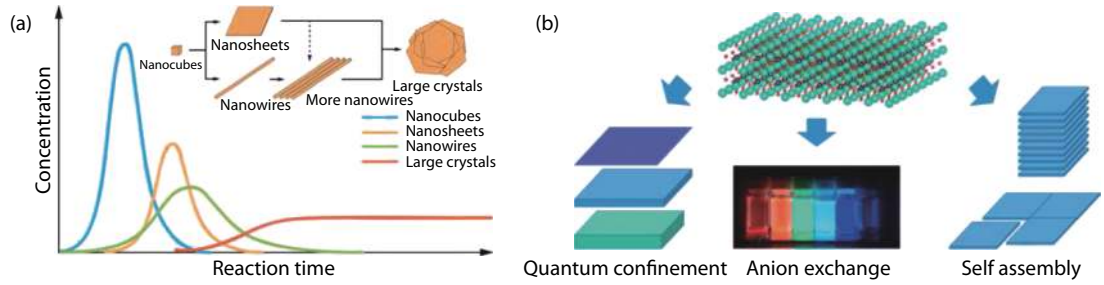

Fig. 8. (Color online) (a) The sketch showing the change of concentration of different species along with time during $CsPbBr_3$ synthesis. Inset: schematic illustration of the morphology evolution during $CsPbBr_3$ synthesis. Reproduced with permission from Ref. [88]. (b) Schematic diagram of the effects of the reaction temperature on tuning the thickness and self-assembly of $CsPbX_3$ nanoplates. Reproduced with permission from Ref. [90].

posed a facile re-precipitation strategy to synthesize 0D spherical $CsPbX_3$ quantum dots, nanocubes, 1D nanorods, and 2D nanoplatelets, and these well-defined morphologies could be tuned by changing the chain lengths of organic acids and amines. The corresponding effects of different amino and carboxylic functional groups in the dimensionality of $CsPbX_3$ NCs are presented in Fig. 7(b). Thus, it can be seen that varying chain lengths and structures of organic surfactants can realize the anisotropic growth of $CsPbX_3$ NCs. Manna group[84] created a facile method to tune the width of $CsPbBr_3$ NWs, from the non-confined regime (10 nm) to strong quantum-confinement regime (3.4 nm), only by introducing carboxylic acids, octanoic acid or hexanoic acid (Fig. 7(c)). These acid ligands with short aliphatic chains were believed to inhibit the growth of some crystallographic facets, while enhancing some other sets of them. Not only the chain length of organic acid, but also that of organic amines could affect the morphology of $CsPbX_3$. Yuan *et al.*[85] selected several organic amines with different chain lengths, oleylamine, cetylamine and octylamine together with oleic acid respectively as surfactants to synthesize a series of $CsPbX_3$ NCs at different temperatures. It was found that the $CsPbBr_3$ NCs synthesized in the presence of short carbon-chain amine had a tendency of low-dimensional growth, leading to the formation of nanoplates and nanosheets at low temperature.

Apart from varying chain lengths and structures, the tuning of the ratio of organic acids to organic amines also plays an important role in the controllable synthesis of $CsPbX_3$ NCs. Deng group succeeded in producing low-dimensional nanosheets and NWs with high yields by simply tuning the ratios of organic amines to acids in the reaction process[86]. The schematic illustration for the formation of perovskite NWs and nanosheets is given in Fig. 7(d). Meanwhile, it was also found that different morphologies could be better distinguished and selected while the bis(2-ethylhexyl)-amine (BEHA) participated in the reaction, and the morphology control may be attributed to different binding kinetics of the two capping agents on each crystal facet.

A similar report on the effects of different OAm to OA ratios on the morphology control was reported by Liang and co-workers as well[87]. Accordingly, the shapes of the as-obtained $CsPbBr_3$ NCs with bright blue emission could be systematically engineered into single and lamellar-structured 0D quantum dots, as well as face-to-face stacking 2D nanoplatelets and flat-lying 2D nanosheets via tuning the ratios of OA to OAm. Consistent with other studies, the claimed internal mechanism was the growth rate of different crystal facets of $CsPbBr_3$ NCs due to the preferential crystal facets under the existence of different surfactants.

4.2. Effects of the reaction time

Reaction time is a crucial and effective parameter to regulate the growth and shape of NCs. As to the colloidal synthesis of $CsPbX_3$ NCs, the growth and formation usually take a quite short time even within several seconds[24]. To study the evolution of the $CsPbX_3$ NCs with reaction time prolonging, the Yang group conducted a series of pioneering work[88]. They carefully investigated the formation dynamics of $CsPbX_3$ NCs by reacting cesium oleate with PbX_2 in a hot solvent of ODE with OAm and OA at 150–250 °C and analyzed the intermediates at different reaction times. The formation sketch at 150 °C is illustrated in Fig. 8(a). They found that the initial products (when $t < 10$ min) were mainly composed of the $CsPbX_3$ nanocubes with size ranging from 3 to 7 nm. After 10 min, a few thin NWs with diameters around 9 nm were found in the products. With the reaction time increasing, more NWs were formed but the amount of the nanocubes was decreased, while some large square-shaped nanosheeet appeared. At a later formation stage (40–60 min) of the reaction, the nanosheets dissolved, and the products were dominated by NWs with diameters uniformly below 12 nm and lengths up to 5 μm. The uniform NWs stably existed until the reaction time exceeding 90 min and the main products of irregular large particles were finally found. Noticeably, these intermediate morphologies coexisted with each other instead of independent presence. This observation distinctly revealed the impacts of reaction time on the morphology evolution of $CsPbX_3$ NCs. The similar growth process was also observed in the lead-free inorganic perovskite analogue NCs. For the first time, Deng group[78] successfully synthesized different-shaped Cs_2SnI_6 NCs by a modified traditional hot-injection protocol under argon atmosphere. After the injection of Cs-precursor within 1 min, most of the samples were found to be spherical quantum dots with an average diameter of 2.5 nm. Further increasing the reaction time led to the formation of nanorods, which were dominated over the products. Then the nanorods progressively evolved into longer NWs. With reaction time reaching 30 min, the NWs assembled side-by-side to form nanobelts, which were finally transformed into nanoplates with a thickness of around 8 nm. The aforementioned results indicated that low-dimensional nanostructures such as quantum dot, nanocubes were

the preferable products in the shorter reaction time. With the extension of the reaction time, the dominant morphologies tended to be 1D NWs or nanorods and 2D nanoplates and nanosheets.

4.3. Effects of the reaction temperature

For the traditional hot-injection method, the reaction temperature is one of the key parameters in controllable synthesis of $CsPbX_3$ NCs[89]. Alivisatos group reported a controllable synthesis of $CsPbX_3$ NCs, and the shape could be tuned from nanoplatelets to nanocubes via changing the reaction temperature from 90 to 150 °C (Fig. 8(b))[90]. In this work, green-emitting $CsPbBr_3$ nanocubes were produced under a higher reaction temperature of 150 °C. In contrast, cyan-emitting nanoplatelets and blue-emitting nanoplatelets were obtained at lower temperatures of 130 and 90 °C, respectively. This result revealed that the lower temperature had a favorable impact on the formation of anisotropic nanostructures. Similar results are also observed in other reports[85, 88].

4.4. Dimensional-control through tuning the reaction parameters

Generally speaking, the general morphologies of inorganic halide perovskites NCs can be divided into 0D nanospheres (quantum dots) and nanocubes, 1D NWs and nanorods, plus 2D nanoplates and nanosheets. Since the shapes of NCs are in close association with the further utilization in different optoelectronic fields, the dimension-controllable synthesis of inorganic perovskite NCs has been a hot spot.

The 0D nanocubes and nanospheres are the most commonly achieved morphologies through a traditional hot-injection method with longer organic ligands at a relatively high temperature for short reaction time. The size-control of nanocubes can be easily realized by tuning the OAm/OA ratios[86, 87], reaction temperatures[85, 88, 90] and the concentration of precursors[26]. As for nanospheres, similar synthetic methods can also be employed. $CsPbBr_3$ nanospheres with an average diameter of 2.4 nm were firstly reported through the hot-injection method with a OA to OAm ratio of 0.6 : 0.3 at 90 °C[87]. The ultra-small $CsPbX_3$ nanospheres with a nearly amorphous structure can also be obtained at very low reaction temperatures (0 °C)[36]. Organic surfactants with shorter chain lengths have been successfully used to produce $CsPbX_3$ nanospheres with an average diameter of 4.3 nm as well[83].

1D NWs and nanorods are widely used in some specific optoelectronic applications, such as photodetectors and lasers. In contrast to the 0D nanospheres and nanocubes, the formation of 1D NWs usually takes a longer reaction time. The pioneering work of 1D $CsPbX_3$ NWs was reported by the Yang group[88], and the 1D NWs were obtained by prolonging reaction time up to 1 h, in which the morphology of the NCs changed from nanocubes to large nanoparticles. Fine-tuning capping ligands could also assist the formation of anisotropic NWs by selective binding to certain crystal facets[84]. Single-crystalline $CsPbBr_3$ NWs were able to directly form precursor powders with controllable length and width by regulating the reaction time[91]. Additionally, extra adding of hydrohalic acids (HX, X = Cl, Br, I) could affect the length of $CsPbX_3$ NWs[92]. On the other hand, however, studies on $CsPbX_3$ nanorods are still very limited. The $CsPbX_3$ nanorods with the length of 200 nm were firstly synthesized via a ligand-mediated process using acetate acid and dodecylamine[83]. Another example of successful production of the uniform rod-shaped structure was hybrid halide $CsPb(Br/I)_3$ nanorods through a modified hot-injection method[93].

The 2D $CsPbX_3$ nanoplates and nanosheets have attracted much attention due to their unique structures and outstanding properties as future promising candidates for optoelectronic devices. In general, lower reaction temperatures and hybrid short and long ligands tend to generate the formation of nanoplates and nanosheets. This discovery has been firmly ensured by many groups[82, 85, 90, 94, 95]. Besides, the polarity of solvents is found to play a significant role in the morphology evolution from nanocubes to nanoplates, and further to nanobars[96, 97]. What's more, the introduction of additional metal halides as models to induce the self-assembly of nanorods into nanoplates has been reported as well[98].

5. Strategies for stability improvement

One of the most challenging obstacles to the practical application of perovskite NCs lies in their inherent poor photo- and thermo-stability, and they have been proven to easily degrade in the presence of oxygen and moisture. Compared with hybrid organic-inorganic halide perovskites, all-inorganic $CsPbX_3$ NCs are endowed with relatively better stability. However, the intrinsic ionic character still hinders their further utilization in many fields. Hence, to overcome these stability problems, many strategies have been developed to passivate the unstable surfaces, mainly including surface modification by organic ligands or inorganic chemicals and encapsulation in some stable shells or water-proof materials.

The traditionally used organic amines and organic acids can not only control over the morphology, but also protect the surface and enhance the stability. Except for the most used OAm and OA, sorts of branched capping ligands have been employed due to their strong steric effect. For example, trioctylphosphine (TOP)[99], trioctylphosphine oxide (TOPO)[100], bis-(2,2,4-trimethylpentyl) phosphinic acid (TMPPA)[101], di-dodecyl dimethyl ammonium bromide (DDAB)[102] along with hybrid S^{2-} and DDA^+ ion pair[103] and so on, have been introduced to passivate the surface of $CsPbX_3$ NCs either by *in-situ* capping or post-synthetic ligand exchange methods, which facilitate the stability in air and polar solvents, as well as enhancing the optical properties. Moreover, the organic surfactants can be *in-situ* carbonized on the surface via X-ray treatment, resulting in intensive protection against easy removal and dissolution[104]. The improvement of stability can be realized by the introduction of inorganic chemicals coating on the surface. According to previous reports, the $PbBr_2$-rich surface favored the increase of PLQY and improvement of stability, thus the post-treatment process was conducted by using $PbBr_2$[105, 106], $ZnBr_2$[107, 108] and HBr[109] etc. as resources. In addition, inorganic anions K^+[110] and Ag^+[111] were also introduced to passivate surfaces.

Apart from the surface treatment with organic or inorganic surfactants, the encapsulation of $CsPbX_3$ NCs into more stable materials is another feasible strategy to improve the stability. Silicon is commonly used as protective coating shells: mesoporous silica was used as a template to assist the formation of $CsPbX_3$ NCs, and the as-synthesized $CsPbX_3$ powders exhibited high PL efficiencies along with improved stability[40].

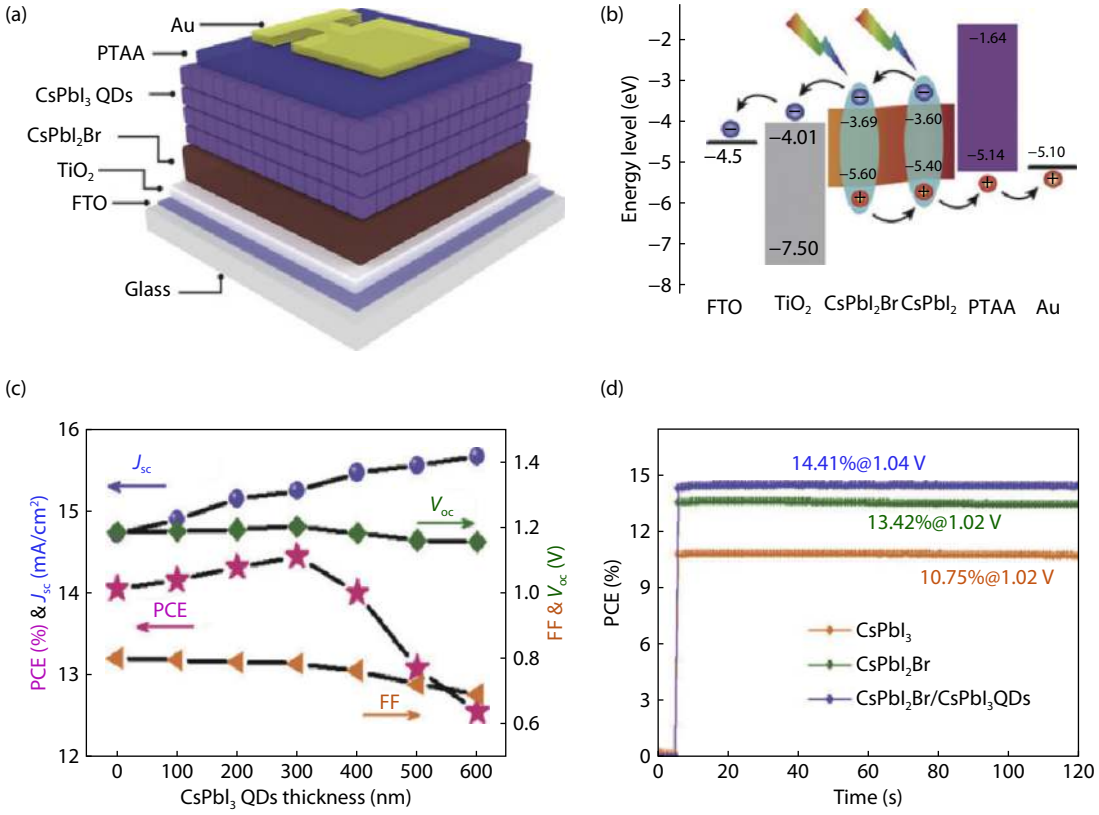

Fig. 9. (Color online) (a) The structure illustration of $CsPbI_{2+x}Br_{1-x}$ perovskite solar cell using $CsPbBrI_2$ and $CsPbI_3$ quantum dots (QDs) as component cells. (b) The halide-ion-profiled heterojunction designed at the $CsPbBrI_2/CsPbI_3$ QD interface to achieve proper band-edge. (c) The optimization of $CsPbI_3$ QD layer in the graded bandgap structure to achieve maximum overall light harvesting. (d) The remarkable PCE of the as-fabricated device. Reproduced with permission [153].

Effective $CsPbX_3$ NCs/SiO_2 nanocomposites were obtained by directly mixing the $CsPbX_3$ NCs with mesoporous SiO_2 with pore sizes of 12–15 nm[112]. The SiO_2 coated $CsPbX_3$ composites were also achieved through *in-situ* decoration of (3-aminopropyl)triethoxysilane (APTES)[113] and NH_2-polyhedral oligomeric silsesquioxane (NH_2-POSS)[114]. Moreover, another facile sol-gel method was also utilized to prepare the monodisperse $CsPbX_3/SiO_2$ core/shell nanostructures. What's more, other oxides or sulfides, including Al_2O_3[115], TiO_2[116], MoS_2[117] and ZnS[118], were also utilized in the encapsulation process. Furthermore, the versatile carbon materials, such as graphene[119] and nanotubes[120] were both promising modified candidates in further application. Polymer coating shells were also regarded as efficient stabilization way due to their outstanding hydrophobic features. Polystyrene (PS) beads[121] and fibers[122] were applied as capsule shells against exposure to water and thermal treatment. Besides, poly(methyl methacrylate) (PMMA)[123] and polyvinyl pyrrolidone (PVP)[124] encapsulation were also utilized in LEDs devices, and poly(maleic anhydride-alt-1-octadecene) (PMA) capping agent was also proved to efficiently prevent $CsPbX_3$ from aggregation by tightening the superficial ligand bindings[125, 126].

6. Optoelectronic applications

The all-inorganic metal halide perovskite is no doubt one of the most promising materials emerging in recent years, and it can be clearly foreseen that this booming material is still equipped with great development potentials. The highly ionic features endow $CsPbX_3$ NCs with defect-tolerance, which consequently results in high PLQYs and narrow full width at half maximum (FWHM)[127, 128]. Additionally, their PL emission can be tuned simply by changing the halide composition and their bandgap is insensitive to the temperature, quite different from traditional metal chalcogenide and pnictide NCs[26, 129]. Thanks to all these excellent optoelectronic properties, $CsPbX_3$ NCs are very perspective in various applications including solar cells[130–134], light-emitting diodes (LEDs)[119, 135–137], photodetectors (PDs)[138–141], lasers[29, 142–144], photocatalysis[119, 145, 146] and field-effect transistors (FETs)[147–149].

Perovskite solar cells, especially organic-inorganic hybrid ones are widely investigated and the power conversion efficiency (PCE) has reached 23.3% in 2019[150]. Compared with hybrid solar cells, which suffer from the problem of instability, $CsPbX_3$ NCs are more thermally stable and temperature insensitive. The cubic phase of $CsPbX_3$ NCs is crucial to acquire suitable band gap for achieving high PCE[133, 134]. Researchers have discovered that introducing bromide into crystal lattice or introducing some surfactants to the surface by post-treatment will help stabilize the cubic phase of $CsPbI_3$[151, 152]. The optimal PCEs obtained through the aforementioned two methods could reach 9.8% and 13.4%, respectively. Besides, to form a thin and compact inorganic lead oxysalt layer on the perovskite surface is also an efficient general strategy to enhance the PCE efficiency[153]. A higher PCE of 14.5% for $CsPbX_3$ was obtained via compressing $CsPbI_3/CsPbI_2Br$ bilayers together to form a tandem solar cell[154], as is shown in Fig. 9. Very recently, a tetragonal β-phase of $CsPbI_3$ was reported,

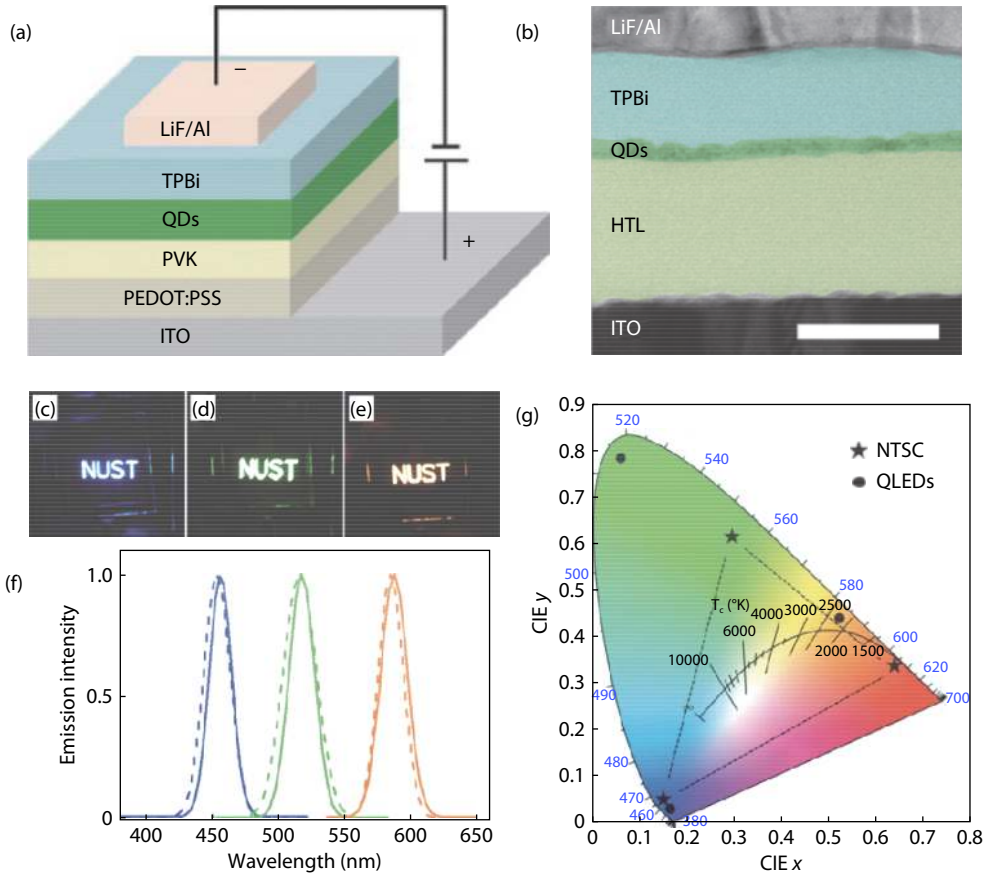

Fig. 10. (Color online) (a) Schematic illustration and (b) cross-sectional TEM image of an LED device. (c-e) Photographs and (f) EL spectra (straight line) of LED devices with different halide compositions, and the PL spectra (dashed line) of NCs dispersed in hexane. (g) The Commission Internationale del'Eclairage (CIE) coordinates of the three-color QLEDs (circular) compared to the National Television System Committee (NTSC) color standards (stars). Reproduced with permission from Ref. [155].

which exhibited higher stability and a more favorable bandgap[155]. This material allowed for PCEs of 18% after the passivation of the surface trap state with choline iodide. Although PCEs of $CsPbX_3$ are still far away from that of hybrid solar cells, the rapid growing efficiency and environmental stability clarify the bright prospects of $CsPbX_3$ NCs as the next-generation solar cells materials.

Taking advantage of their wide and tunable emission wavelength, $CsPbX_3$ NCs have drawn great attention in the applications of lightening and display as backlight LEDs. Many efforts have been made from three aspects including carrier injection efficiency, radiative recombination efficiency and injection balance to improve performance and stability of LEDs[56, 102, 156]. The first electrically driven $CsPbX_3$ NCs based LED was reported by the Zeng group (Fig. 10)[157]. The external quantum efficiency (EQE) increases from less than one 1% to 16.48% within three years[147], exhibiting an ultrafast progressing speed. To the best of our knowledge, currently, the highest EQE of inorganic perovskite quantum-dot LEDs involved of $CsPbX_3$ NCs has exceeded 20% by mixing presynthesized $CsPbBr_3$ perovskite NCs with MABr additives as the passivation layer[148]. In spite of remarkable development achieved, the practical application of the $CsPbX_3$ NCs-based LEDs is still challenging as EQE of blue LED is just around 0.1%, which is far away from the prerequisite to produce white LEDs[94, 109].

In a reverse process, the PDs should extract photo-generated carriers quickly and efficiently to ensure ultrafast response and high turn/off ratio. The high absorption efficiency (2×10^5 cm^{-1})[46] and large carrier mobility[109] enable $CsPbX_3$ NCs a potential candidate for light detection. Aligned films of $CsPbI_3$ NCs displayed excellent photosensitivity (on/off ratio of 105) and fast response speed (rise time of 24 ms and decay time of 29 ms)[139]. Besides, the 2D $CsPbBr_3$ NCs are preferable for fabricating large-area and crack-free planar films[149]. The ultrathin and flexible PDs showed a detectable limit of 21.5 pW/cm^2 and a fast response time of 20 ns, implying its promising application in flexible devices (Fig. 11(a))[140].

Very recently, the $CsPbX_3$ NCs were found to be efficient catalysts for photocatalytic CO_2 reduction. $CsPbBr_3$ was reported to be utilized in the CO_2 reduction to produce the mono-carbon product with nearly one-unit selectivity (Fig. 11(b))[119, 145]. It is undoubtedly that high absorption coefficient, high charge carrier mobility and long charge diffusion length of $CsPbX_3$ are very beneficial for light-harvesting and charge migration to the active center. Problems left are the instability of $CsPbX_3$ in aqueous solution and the use of highly toxic element lead in $CsPbX_3$ NCs. Further efforts should be devoted to developing environmental benignly IHP NCs for photocatalytic applications[146].

The unique optical features of high PLQYs, tunable emission and temperature insensitive also render $CsPbX_3$ NCs as the ideal gain media for constructing laser devices via coup-

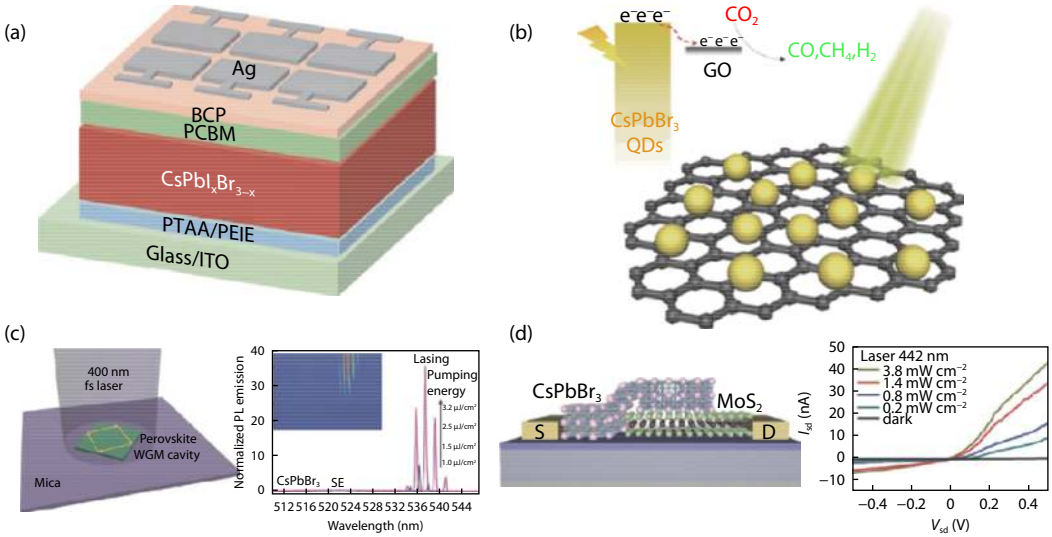

Fig. 11. (Color online) (a) Schematic structure of photodetector based on all–inorganic perovskite $CsPbI_xBr_{3-x}$. Reproduced with permission from Ref. [140]. (b) Schematic diagram of CO_2 photoreduction over the $CsPbBr_3$ QD/GO photocatalyst. Reproduced with permission from Ref. [119]. (c) Schematic of a $CsPbX_3$ (X = Cl, Br, or I) plate on mica substrate pumped by a 400 nm laser excitation. On the right are the emission spectra at five different optical pump fluencies, showing the transition from spontaneous emission to amplified spontaneous emission and to lasing. Inset: 2D pseudo–color plot of the plate emission spectra under different pump fluence (P). Reproduced with permission from Ref. [144]. (d) Schematic illustration of the $CsPbBr_3/MoS_2$ heterojunction phototransistor. On the right is the comparison of I_{sd}–V_{sd} characteristics of this heterojunction in darkness and under a 442 nm laser with different intensities. Reproduced with permission from Ref. [160].

ling with another optical cavity[29]. The best $CsPbX_3$ NCs-base lasing devices displayed a threshold as low as 2.1 μJ/cm^2 with multicolor (400–700 nm) (Fig. 11(c))[144]. Low threshold, high-quality factor and adjustable multicolor make $CsPbX_3$ NCs hopeful gain media in lasing devices.

Except for the above optoelectronic applications, the $CsPbX_3$ NCs can also be utilized in field-effect transistors (FETs) due to their large charge carrier mobility[158] and ambipolar conductivity[159]. Moreover, quite different from the traditional silicon semiconductors, perovskite thin films are flexible, endowing it with great potential in stretchable and wearable electronics. Besides, combining $CsPbBr_3$ NCs and 2D semiconductor materials, such as MoS_2, to form heterojunctions is also a potential excellent strategy to design high-performance phototransistors (Fig. 11(d))[160]. An obstacle that prohibits its wide investigation of perovskite-based FETs lies in the gate-field screening effect resulting from ion migration[161]. Various methods including optimizing perovskite microstructures, using less polar cations in perovskites, or using external light excitation for ion migration compensation have been employed to solve the problems[162].

7. Summary and outlook

In this review, recent advances on representative fabrication methods of all-inorganic halide perovskite NCs and their related applications have been summarized, especially focusing on the controllable synthesis methods and parameter regulation. Despite remarkable achievements obtained in the past four years, there still exist many issues to be addressed and plenty of challenges to be defeated before realizing the practical application of $CsPbX_3$ NCs.

The most intractable problem is their poor stability against moisture, oxygen, heat and persistent light irradiation. The ionic nature of $CsPbX_3$ NCs decides that they are very sensitive to the polar solvents such as water, consequently restrict their applications in many areas. Continuous heat or light irradiation would cause detachment of surface ligands at elevated temperatures, which are crucial for protecting $CsPbX_3$ NCs from aggregation and the formation of carrier traps. Common methods used to address these two issues are surface coating, ligand treatment, and the introduction of a host matrix. Inert shells such as aluminum oxide and silica have been found to effectively improve resistance of $CsPbX_3$ NCs to moisture and light irradiation[115]. Carbonized surface ligands created by low-flux X-ray irradiation are also reported to effectively protect the $CsPbX_3$ from water and air[104]. The implant of $CsPbX_3$ onto silica or into polymer will prohibit the NCs from aggregation thus improving their stability[121–124]. Although the aforementioned techniques have been developed and great progress has been made, it is still challenging to stabilize the $CsPbX_3$ NCs without affecting their optoelectronic properties. Moreover, much attention has been made to stabilizing the green-emitting $CsPbBr_3$ NCs. Other $CsPbX_3$ NCs are waiting to be investigated and protected.

It is well known that lead in $CsPbX_3$ NCs is toxic to health, which prevents $CsPbX_3$ NCs from practical application and commercialization. Some eco-friendly elements including tin (Sn), bismuth (Bi), germanium (Ge), indium (In), and antimony (Sb) have been investigated as alternatives to lead[163, 164]. However, these lead-free perovskite NCs display much lower PLQY (less than 1%) compared with $CsPbX_3$ NCs, which make them unfavorable for optoelectronic applications. Furthermore, these substitutions are less stable and can be easily oxidized in the air[78]. More efforts should be devoted to developing lead-free all-inorganic perovskite NCs with satisfactory optoelectronic properties.

It is worth noting that the commonly used core-shell structure in metal-chalcogenide quantum dots is not feasible for

all-inorganic perovskite NCs because of the spontaneous anion-exchange reactions. However, coating the all-inorganic perovskite NCs with traditional metal-chalcogenides to form a core-shell heterostructure not only can serve as protection layer against air and moisture, but also can tune their optoelectronic properties for various applications. On the other hand, the adoption of this core-shell heterostructure owns the potential to radically circumvent fast Auger recombination, which will undoubtedly improve the efficiency of all-inorganic perovskite NCs in high flux applications[165].

In conclusion, more efforts should be contributed to explore effective methods for all-inorganic perovskite NCs stabilization while preserving their optoelectronic property. The exploitation of lead-free all-inorganic halide perovskite NCs with comparable efficiency is also highly urgent for their commercialization. The creation of some core-shell heterostructures coupled with traditional metal chalcogenides is a promising approach for developing high flux all-inorganic halide perovskite NCs. We believe that the all-inorganic halide perovskite NCs will emerge as a new class of fascinating optoelectronic materials and hold a bright future for various applications.

Acknowledgments

This work was supported by the Fundamental Research Funds for the Central Universities (No.2019RC020).

References

[1] Alivisatos A P. Semiconductor clusters, nanocrystals, and quantum dots. Science, 1996, 271, 933
[2] El-Sayed M A. Small is different: shape-, size-, and composition-dependent properties of some colloidal semiconductor nanocrystals. Acc Chem Res, 2004, 37, 326
[3] Carey G H, Abdelhady A L, Ning Z, et al. Colloidal quantum dot solar cells. Chem Rev, 2015, 115, 12732
[4] Li L, Hu J, Yang W, et al. Band gap variation of size- and shape-controlled colloidal CdSe quantum rods. Nano Lett, 2001, 1, 349
[5] Peng X, Manna L, Yang W, et al. Shape control of CdSe nanocrystals. Nature, 2000, 404, 59
[6] Kagan C R, Lifshitz E, Sargent E H, et al. Building devices from colloidal quantum dots. Science, 2016, 353, 5523
[7] Caruge J M, Halpert J E, Wood V, et al. Colloidal quantum-dot light-emitting diodes with metal-oxide charge transport layers. Nat Photon, 2008, 2, 247
[8] Shirasaki Y, Supran G J, Bawendi M G, et al. Emergence of colloidal quantum-dot light-emitting technologies. Nat Photon, 2013, 7, 13
[9] Kovalenko M V, Protesescu L, Bodnarchuk M I. Properties and potential optoelectronic applications of lead halide perovskite nanocrystals. Science, 2017, 358, 745
[10] Amgar D, Aharon S, Etgar L. Inorganic and hybrid organo-metal perovskite nanostructures: synthesis, properties, and applications. Adv Funct Mater, 2016, 26, 8576
[11] Stoumpos C C, Kanatzidis M G. The renaissance of halide perovskites and their evolution as emerging semiconductors. Acc Chem Res, 2015, 48, 2791
[12] Kojima A, Teshima K, Shirai Y, et al. Organometal halide perovskites as visible-light sensitizers for photovoltaic cells. J Am Chem Soc, 2009, 131, 6050
[13] Grätzel M. The light and shade of perovskite solar cells. Nat Mater, 2014, 13, 838
[14] Yang W S, Noh J H, Jeon N J, et al. High-performance photovoltaic perovskite layers fabricated through intramolecular exchange. Science, 2015, 348, 1234
[15] Green M A, Ho-Baillie A, Snaith H J. The emergence of perovskite solar cells. Nat Photon, 2014, 8, 506
[16] Jiang Q, Zhao Y, Zhang X, et al. Surface passivation of perovskite film for efficient solar cells. Nat Photon, 2019, 13, 460
[17] Xiao Z, Kerner R A, Zhao L, et al. Efficient perovskite light-emitting diodes featuring nanometre-sized crystallites. Nat Photon, 2017, 11, 108
[18] Zhao Y, Zhu K. Organic-inorganic hybrid lead halide perovskites for optoelectronic and electronic applications. Chem Soc Rev, 2016, 45, 655
[19] Jeon N J, Noh J H, Kim Y C, et al. Solvent engineering for high-performance inorganic-organic hybrid perovskite solar cells. Nat Mater, 2014, 13, 897
[20] Smith I C, Hoke E T, Solis-Ibarra D, et al. A layered hybrid perovskite solar-cell absorber with enhanced moisture stability. Angew Chem Int Ed, 2014, 53, 11232
[21] Liang J, Wang C, Wang Y, et al. All-inorganic perovskite solar cells. J Am Chem Soc, 2016, 138, 15829
[22] Shi Z, Li S, Li Y, et al. Strategy of solution-processed all-inorganic heterostructure for humidity/temperature-stable perovskite quantum dot light-emitting diodes. ACS Nano, 2018, 12, 1462
[23] Stoumpos C C, Malliakas C D, Peters J A, et al. Crystal growth of the perovskite semiconductor $CsPbBr_3$: a new material for high-energy radiation detection. Cryst Growth Des, 2013, 13, 2722
[24] Li X, Cao F, Yu D, et al. All inorganic halide perovskites nanosystem: synthesis, structural features, optical properties and optoelectronic applications. Small, 2017, 13, 1603996
[25] Ahmad W, Khan J, Niu G, et al. Inorganic $CsPbI_3$ perovskite-based solar cells: A choice for a tandem device. Solar RRL, 2017, 1, 1700048
[26] Protesescu L, Yakunin S, Bodnarchuk M I, et al. Nanocrystals of cesium lead halide perovskites ($CsPbX_3$, X = Cl, Br, and I): novel optoelectronic materials showing bright emission with wide color gamut. Nano Lett, 2015, 15, 3692
[27] Yang D, Cao M, Zhong Q, et al. All-inorganic cesium lead halide perovskite nanocrystals: synthesis, surface engineering and applications. J Mater Chem C, 2019, 7, 757
[28] Huo C, Cai B, Yuan Z, et al. Two-dimensional metal halide perovskites: theory, synthesis, and optoelectronics. Small Methods, 2017, 1, 1600018
[29] Wang Y, Li X, Song J, et al. All-inorganic colloidal perovskite quantum dots: a new class of lasing materials with favorable characteristics. Adv Mater, 2015, 27, 7101
[30] Veldhuis S A, Boix P P, Yantara N, et al. Perovskite materials for light-emitting diodes and lasers. Adv Mater, 2016, 28, 6804
[31] Wells H L. Über die Cäsium-und Kalium-Bleihalogenide. Zeitschrift für anorganische Chemie, 1893, 3, 195
[32] Møller C K. A phase transition in cæsium plumbochloride. Nature, 1957, 180, 981
[33] Yarema M, Yarema O, Lin W M M, et al. Upscaling colloidal nanocrystal hot-injection syntheses via reactor underpressure. Chem Mater, 2017, 29, 796
[34] Chen X, Peng L, Huang K, et al. Non-injection gram-scale synthesis of cesium lead halide perovskite quantum dots with controllable size and composition. Nano Res, 2016, 9, 1994
[35] Zhang F, Zhong H, Chen C, et al. Brightly luminescent and color-tunable colloidal $CH_3NH_3PbX_3$ (X = Br, I, Cl) quantum dots: potential alternatives for display technology. ACS Nano, 2015, 9, 4533
[36] Li X, Wu Y, Zhang S, et al. $CsPbX_3$ quantum dots for lighting and displays: room-temperature synthesis, photoluminescence superiorities, underlying origins and white light-emitting diodes. Adv Funct Mater, 2016, 26, 2435
[37] Tong Y, Bladt E, Aygüler M F, et al. Highly luminescent cesium lead halide perovskite nanocrystals with tunable composition

and thickness by ultrasonication. Angew Chem Int Ed, 2016, 55, 13887

[38] Li X, Liu Y, Song X, et al. Intercrossed carbon nanorings with pure surface states as low-cost and environment-friendly phosphors for white-light-emitting diodes. Angew Chem Int Ed, 2015, 54, 1759

[39] Li J, Xu L, Wang T, et al. 50-fold EQE improvement up to 6.27% of solution-processed all-inorganic perovskite $CsPbBr_3$ QLEDs via surface ligand density control. Adv Mater, 2017, 29, 1603885

[40] Dirin D N, Protesescu L, Trummer D, et al. Harnessing defect-tolerance at the nanoscale: highly luminescent lead halide perovskite nanocrystals in mesoporous silica matrixes. Nano Lett, 2016, 16, 5866

[41] Pan Q, Hu H, Zou Y, et al. Microwave-assisted synthesis of high-quality "all-inorganic" $CsPbX_3$ (X = Cl, Br, I) perovskite nanocrystals and their application in light emitting diodes. J Mater Chem C, 2017, 5, 10947

[42] Niu G, Ruditskiy A, Vara M, et al. Toward continuous and scalable production of colloidal nanocrystals by switching from batch to droplet reactors. Chem Soc Rev, 2015, 44, 5806

[43] Lignos I, Stavrakis S, Nedelcu G, et al. Synthesis of cesium lead halide perovskite nanocrystals in a droplet-based microfluidic platform: fast parametric space mapping. Nano Lett, 2016, 16, 1869

[44] Liao H, Guo S, Cao S, et al. A general strategy for in situ growth of all-inorganic $CsPbX_3$ (X = Br, I, and Cl) perovskite nanocrystals in polymer fibers toward significantly enhanced water/thermal stabilities. Adv Opt Mater, 2018, 6, 1800346

[45] Zhu Z Y, Yang Q Q, Gao L F, et al. Solvent-free mechanosynthesis of composition-tunable cesium lead halide perovskite quantum dots. J Phys Chem Lett, 2017, 8, 1610

[46] De Roo J, Ibáñez M, Geiregat P, et al. Highly dynamic ligand binding and light absorption coefficient of cesium lead bromide perovskite nanocrystals. ACS Nano, 2016, 10, 2071

[47] Friščić T, Halasz I, Beldon P J, et al. Real-time and in situ monitoring of mechanochemical milling reactions. Nat Chem, 2013, 5, 66

[48] Chen J, Fu Y, Samad L, et al. Vapor-phase epitaxial growth of aligned nanowire networks of cesium lead halide perovskites ($CsPbX_3$, X = Cl, Br, I). Nano Lett, 2016, 17, 460

[49] Nedelcu G, Protesescu L, Yakunin S, et al. Fast anion-exchange in highly luminescent nanocrystals of cesium lead halide perovskites ($CsPbX_3$, X = Cl, Br, I). Nano Lett, 2015, 15, 5635

[50] Akkerman Q A, D'Innocenzo V, Accornero S, et al. Tuning the optical properties of cesium lead halide perovskite nanocrystals by anion exchange reactions. J Am Chem Soc, 2015, 137, 10276

[51] Dou L, Wong A B, Yu Y, et al. Atomically thin two-dimensional organic-inorganic hybrid perovskites. Science, 2015, 349, 1518

[52] D'Innocenzo V, Srimath Kandada A R, De Bastiani M, et al. Tuning the light emission properties by band gap engineering in hybrid lead halide perovskite. J Am Chem Soc, 2014, 136, 17730

[53] Yang H, Zhang Y, Pan J, et al. Room-temperature engineering of all-inorganic perovskite nanocrsytals with different dimensionalities . Chem Mater, 2017, 29, 8978

[54] Wang K H, Wu L, Li L, et al. Large-scale synthesis of highly luminescent perovskite-related $CsPb_2Br_5$ nanoplatelets and their fast anion exchange. Angew Chem Int Ed, 2016, 55, 8328

[55] Ruan L, Lin J, Shen W, et al. Ligand-mediated synthesis of compositionally related cesium lead halide $CsPb_2X_5$ nanowires with improved stability. Nanoscale, 2018, 10, 7658

[56] Zhang X, Xu B, Zhang J, et al. All-inorganic perovskite nanocrystals for high-efficiency light emitting diodes: dual-phase $CsPbBr_3$-$CsPb_2Br_5$ composites. Adv Funct Mater, 2016, 26, 4595

[57] Tang X, Hu Z, Yuan W, et al. Perovskite $CsPb_2Br_5$ microplate laser with enhanced stability and tunable properties. Adv Opt Mater, 2017, 5, 1600788

[58] Li J, Yu Q, He Y, et al. $Cs_2PbI_2Cl_2$, all-inorganic two-dimensional Ruddlesden–Popper mixed halide perovskite with optoelectronic response. J Am Chem Soc, 2018, 140, 11085

[59] Chen D, Wan Z, Chen X, et al. Large-scale room-temperature synthesis and optical properties of perovskite-related Cs_4PbBr_6 fluorophores. J Mater Chem C, 2016, 4, 10646

[60] Saidaminov M I, Almutlaq J, Sarmah S, et al. Pure Cs_4PbBr_6: highly luminescent zero-dimensional perovskite solids. ACS Energy Lett, 2016, 1, 840

[61] Wang Y, Yu D, Wang Z, et al. Solution-grown $CsPbBr_3/Cs_4PbBr_6$ perovskite nanocomposites: toward temperature-insensitive optical gain. Small, 2017, 13, 1701587

[62] Akkerman Q A, Park S, Radicchi E, et al. Nearly monodisperse insulator Cs_4PbX_6 (X = Cl, Br, I) nanocrystals, their mixed halide compositions, and their transformation into $CsPbX_3$ nanocrystals. Nano Lett, 2017, 17, 1924

[63] Liu Z, Bekenstein Y, Ye X, et al. Ligand mediated transformation of cesium lead bromide perovskite nanocrystals to lead depleted Cs_4PbBr_6 nanocrystals. J Am Chem Soc, 2017, 139, 5309

[64] Li G, Wang H, Zhu Z, et al. Shape and phase evolution from $CsPbBr_3$ perovskite nanocubes to tetragonal $CsPb_2Br_5$ nanosheets with an indirect bandgap. Chem Commun, 2016, 52, 11296

[65] Wu L, Hu H, Xu Y, et al. From nonluminescent Cs_4PbX_6 (X = Cl, Br, I) nanocrystals to highly luminescent $CsPbX_3$ nanocrystals: water-triggered transformation through a CsX-stripping mechanism. Nano Lett, 2017, 17, 5799

[66] Palazon F, Urso C, De Trizio L, et al. Postsynthesis transformation of insulating Cs_4PbBr_6 nanocrystals into bright perovskite $CsPbBr_3$ through physical and chemical extraction of CsBr. ACS Energy Lett, 2017, 2, 2445

[67] Shen W, Ruan L, Shen Z, et al. Reversible light-mediated compositional and structural transitions between $CsPbBr_3$ and $CsPb_2Br_5$ nanosheets. Chem Commun, 2018, 54, 2804

[68] Chung I, Song J H, Im J, et al. $CsSnI_3$: semiconductor or metal? High electrical conductivity and strong near-infrared photoluminescence from a single material. High hole mobility and phase-transitions J Am Chem Soc, 2012, 134, 8579

[69] Udayabhaskararao T, Houben L, Cohen H, et al. A mechanistic study of phase transformation in perovskite nanocrystals driven by ligand passivation. Chem Mater, 2017, 30, 84

[70] Ruan L, Shen W, Wang A, et al. Alkyl-thiol ligand-induced shape- and crystalline phase-controlled synthesis of stable perovskite-related $CsPb_2Br_5$ nanocrystals at room temperature. J Phys Chem Lett, 2017, 8, 3853

[71] Huang L, Lambrecht W R L. Electronic band structure, phonons, and exciton binding energies of halide perovskites $CsSnCl_3$, $CsSnBr_3$, and $CsSnI_3$. Phys Rev B, 2013, 88, 165203

[72] Yang B, Chen J, Hong F, et al. Lead-free, air-stable all-inorganic cesium bismuth halide perovskite nanocrystals. Angew Chem Int Ed, 2017, 56, 12471

[73] Yang F, Hirotani D, Kapil G, et al. All-inorganic $CsPb_{1-x}Ge_xI_2Br$ perovskite with enhanced phase stability and photovoltaic performance. Angew Chem Int Ed, 2018, 57, 12745

[74] Liang J, Liu Z, Qiu L, et al. Enhancing optical, electronic, crystalline, and morphological properties of cesium lead halide by Mn substitution for high-stability all-inorganic perovskite solar cells with carbon electrodes. Adv Energy Mater, 2018, 8, 1800504

[75] Xiao Z, Du K Z, Meng W, et al. Intrinsic instability of $Cs_2In(I)M(III)X_6$ (M = Bi, Sb; X = halogen) double perovskites: a combined density functional theory and experimental study. J Am Chem Soc, 2017, 139, 6054

[76] Xiang S, Li W, Wei Y, et al. The synergistic effect of non-stoichiometry and Sb-doping on air-stable α-$CsPbI_3$ for efficient carbon-based perovskite solar cells. Nanoscale, 2018, 10, 9996

[77] Van der Stam W, Geuchies J J, Altantzis T, et al. Highly emissive divalent-ion-doped colloidal $CsPb_{1-x}M_xBr_3$ perovskite nanocrystals through cation exchange. J Am Chem Soc, 2017, 139, 4087

[78] Wang A, Yan X, Zhang M, et al. Controlled synthesis of lead-free and stable perovskite derivative Cs_2SnI_6 nanocrystals via a facile hot-injection process. Chem Mater, 2016, 28, 8132
[79] Xing G, Kumar M H, Chong W K, et al. Solution-processed tin-based perovskite for near-infrared lasing. Adv Mater, 2016, 28, 8191
[80] Wang A, Guo Y, Muhammad F, et al. Controlled synthesis of lead-free cesium tin halide perovskite cubic nanocages with high stability. Chem Mater, 2017, 29, 6493
[81] Wang Y, Tu J, Li T, et al. Convenient preparation of $CsSnI_3$ quantum dots, excellent stability, and the highest performance of lead-free inorganic perovskite solar cells so far. J Mater Chem A, 2019, 7, 7683
[82] Pan A, He B, Fan X, et al. Insight into the ligand-mediated synthesis of colloidal $CsPbBr_3$ perovskite nanocrystals: the role of organic acid, base, and cesium precursors. ACS Nano, 2016, 10, 7943
[83] Sun S, Yuan D, Xu Y, et al. Ligand-mediated synthesis of shape-controlled cesium lead halide perovskite nanocrystals via reprecipitation process at room temperature. ACS Nano, 2016, 10, 3648
[84] Imran M, Di Stasio F, Dang Z, et al. Colloidal synthesis of strongly fluorescent $CsPbBr_3$ nanowires with width tunable down to the quantum confinement regime. Chem Mater, 2016, 28, 6450
[85] Yuan Y, Liu Z, Liu Z, et al. Photoluminescence and self-assembly of cesium lead halide perovskite nanocrystals: effects of chain length of organic amines and reaction temperature. Appl Surf Sci, 2017, 405, 280
[86] Wang C, Zhang Y, Wang A, et al. Controlled synthesis of composition tunable formamidinium cesium double cation lead halide perovskite nanowires and nanosheets with improved stability. Chem Mater, 2017, 29, 2157
[87] Liang Z, Zhao S, Xu Z, et al. Shape-controlled synthesis of all-inorganic $CsPbBr_3$ perovskite nanocrystals with bright blue emission. ACS Appl Mater Inter, 2016, 8, 28824
[88] Zhang D, Eaton S W, Yu Y, et al. Solution-phase synthesis of cesium lead halide perovskite nanowires. J Am Chem Soc, 2015, 137, 9230
[89] Quan L N, Quintero-Bermudez R, Voznyy O, et al. Highly emissive green perovskite nanocrystals in a solid state crystalline matrix. Adv Mater, 2017, 29, 1605945
[90] Bekenstein Y, Koscher B A, Eaton S W, et al. Highly luminescent colloidal nanoplates of perovskite cesium lead halide and their oriented assemblies. J Am Chem Soc, 2015, 137, 16008
[91] Liu Y, Guo M, Dong S, et al. Room temperature colloidal synthesis of $CsPbBr_3$ nanowires with tunable length, width and composition. J Mater Chem C, 2018, 6, 7797
[92] Amgar D, Stern A, Rotem D, et al. Tunable length and optical properties of $CsPbX_3$ (X = Cl, Br, I) nanowires with a few unit cells. Nano Lett, 2017, 17, 1007
[93] Tang X, Zu Z, Shao H, et al. All-inorganic perovskite $CsPb(Br/I)_3$ nanorods for optoelectronic application. Nanoscale, 2016, 8, 15158
[94] Yang D, Zou Y, Li P, et al. Large-scale synthesis of ultrathin cesium lead bromide perovskite nanoplates with precisely tunable dimensions and their application in blue light-emitting diodes. Nano Energy, 2018, 47, 235
[95] Shamsi J, Dang Z, Bianchini P, et al. Colloidal synthesis of quantum confined single crystal $CsPbBr_3$ nanosheets with lateral size control up to the micrometer range. J Am Chem Soc, 2016, 138, 7240
[96] Seth S, Samanta A. A facile methodology for engineering the morphology of $CsPbX_3$ perovskite nanocrystals under ambient condition. Sci Rep, 2016, 6, 37693
[97] Li G, Wang H, Zhang T, et al. Solvent-polarity-engineered controllable synthesis of highly fluorescent cesium lead halide perovskite quantum dots and their use in white light-emitting diodes. Adv Funct Mater, 2016, 26, 8478
[98] Li Z J, Hofman E, Davis A H, et al. General strategy for the growth of $CsPbX_3$ (X = Cl, Br, I) perovskite nanosheets from the assembly of nanorods. Chem Mater, 2018, 30, 3854
[99] Wang H, Sui N, Bai X, et al. Emission recovery and stability enhancement of inorganic perovskite quantum dots. J Phys Chem Lett, 2018, 9, 4166
[100] Wu L, Zhong Q, Yang D, et al. Improving the stability and size tunability of cesium lead halide perovskite nanocrystals using trioctylphosphine oxide as the capping ligand. Langmuir, 2017, 33, 12689
[101] Wang C, Chesman A S R, Jasieniak J J. Stabilizing the cubic perovskite phase of $CsPbI_3$ nanocrystals by using an alkyl phosphinic acid. Chem Commun, 2017, 53, 232
[102] Pan J, Quan L N, Zhao Y, et al. Highly efficient perovskite-quantum-dot light-emitting diodes by surface engineering. Adv Mater, 2016, 28, 8718
[103] Pan J, Sarmah S P, Murali B, et al. Air-stable surface-passivated perovskite quantum dots for ultra-robust, single-and two-photon-induced amplified spontaneous emission. J Phys Chem Lett, 2015, 6, 5027
[104] Palazon F, Akkerman Q A, Prato M, et al. X-ray lithography on perovskite nanocrystals films: from patterning with anion-exchange reactions to enhanced stability in air and water. ACS Nano, 2015, 10, 1224
[105] Wang Y, Zhi M, Chang Y Q, et al. Stable, ultralow threshold amplified spontaneous emission from $CsPbBr_3$ nanoparticles exhibiting trion gain. Nano Lett, 2018, 18, 4976
[106] Bohn B J, Tong Y, Gramlich M, et al. Boosting tunable blue luminescence of halide perovskite nanoplatelets through postsynthetic surface trap repair. Nano Lett, 2018, 18, 5231
[107] Woo J Y, Kim Y, Bae J, et al. Highly stable cesium lead halide perovskite nanocrystals through in situ lead halide inorganic passivation. Chem Mater, 2017, 29, 7088
[108] Li F, Liu Y, Wang H, et al. Postsynthetic surface trap removal of $CsPbX_3$ (X = Cl, Br, or I) quantum dots via a ZnX_2/hexane solution toward an enhanced luminescence quantum yield. Chem Mater, 2018, 30, 8546
[109] Wu Y, Wei C, Li X, et al. In situ passivation of $PbBr_6^{4-}$ octahedra toward blue luminescent $CsPbBr_3$ nanoplatelets with near 100% absolute quantum yield. ACS Energy Lett, 2018, 3, 2030
[110] Huang S, Wang B, Zhang Q, et al. Postsynthesis potassium-modification method to improve atability of $CsPbBr_3$ perovskite nanocrystals. Adv Opt Mater, 2018, 6, 1701106
[111] Lu M, Zhang X, Bai X, et al. Spontaneous silver doping and surface passivation of $CsPbI_3$ perovskite active layer enable light-emitting devices with an external quantum efficiency of 11.2%. ACS Energy Lett, 2018, 3, 1571
[112] Wang H C, Lin S Y, Tang A C, et al. Mesoporous silica particles integrated with all-inorganic $CsPbBr_3$ perovskite quantum-dot nanocomposites (MP-PQDs) with high stability and wide color gamut used for backlight display. Angew Chem Int Ed, 2016, 55, 7924
[113] Sun C, Shen X, Zhang Y, et al. Highly luminescent, stable, transparent and flexible perovskite quantum dot gels towards light-emitting diodes. Nanotechnology, 2017, 28, 365601
[114] Luo B, Pu Y C, Lindley S A, et al. Organolead halide perovskite nanocrystals: branched capping ligands control crystal size and stability. Angew Chem Int Ed, 2016, 55, 8864
[115] Loiudice A, Saris S, Oveisi E, et al. $CsPbBr_3$ QD/AlO_x inorganic nanocomposites with exceptional stability in water, light, and heat. Angew Chem Int Ed, 2017, 56, 10696
[116] Zhou L, Yu K, Yang F, et al. All-inorganic perovskite quantum dot/mesoporous TiO_2 composite-based photodetectors with enhanced performance. Dalton Trans, 2017, 46, 1766
[117] Wu H, Kang Z, Zhang Z, et al. Interfacial charge behavior modula-

tion in perovskite quantum dot-monolayer MoS_2 0D-2D mixed-dimensional van der Waals heterostructures. Adv Funct Mater, 2018, 28, 1802015
[118] Chen W, Hao J, Hu W, et al. Enhanced stability and tunable photoluminescence in perovskite $CsPbX_3$/ZnS quantum dot heterostructure. Small, 2017, 13, 1604085
[119] Xu Y F, Yang M Z, Chen B X, et al. A $CsPbBr_3$ perovskite quantum dot/graphene oxide composite for photocatalytic CO_2 reduction. J Am Chem Soc, 2017, 139, 5660
[120] Li X, Yu D, Chen J, et al. Constructing fast carrier tracks into flexible perovskite photodetectors to greatly improve responsivity. ACS Nano, 2017, 11, 2015
[121] Wei Y, Deng X, Xie Z, et al. Enhancing the stability of perovskite quantum dots by encapsulation in crosslinked polystyrene beads via a swelling-shrinking strategy toward superior water resistance. Adv Funct Mater, 2017, 27, 1703535
[122] Wang Y, Zhu Y, Huang J, et al. $CsPbBr_3$ perovskite quantum dots-based monolithic electrospun fiber membrane as an ultrastable and ultrasensitive fluorescent sensor in aqueous medium. J Phys Chem Lett, 2016, 7, 4253
[123] Zhang M, Wang M, Yang Z, et al. Preparation of all-inorganic perovskite quantum dots-polymer composite for white LEDs application. J Alloy Compd, 2018, 748, 537
[124] Hai J, Li H, Zhao Y, et al. Designing of blue, green, and red $CsPbX_3$ perovskite-codoped flexible films with water resistant property and elimination of anion-exchange for tunable white light emission. Chem Commun, 2017, 53, 5400
[125] Meyns M, Perálvarez M, Heuer-Jungemann A, et al. Polymer-enhanced stability of inorganic perovskite nanocrystals and their application in color conversion LEDs. ACS Appl Mater Inter, 2016, 8, 19579
[126] Hou S, Guo Y, Tang Y, et al. Synthesis and stabilization of colloidal perovskite nanocrystals by multidentate polymer micelles. ACS Appl Mater Inter, 2017, 9, 18417
[127] Guo Y, Wang Q, Saidi W A. Structural stabilities and electronic properties of high-angle grain boundaries in perovskite cesium lead halides. J Phys Chem C, 2017, 121, 1715
[128] Koscher B A, Swabeck J K, Bronstein N D, et al. Essentially trap-free $CsPbBr_3$ colloidal nanocrystals by postsynthetic thiocyanate surface treatment. J Am Chem Soc, 2017, 139, 6566
[129] Swarnkar A, Chulliyil R, Ravi V K, et al. Colloidal $CsPbBr_3$ perovskite nanocrystals: luminescence beyond traditional quantum dots. Angew Chem Int Ed, 2015, 54, 15424
[130] Kulbak M, Cahen D, Hodes G. How important is the organic part of lead halide perovskite photovoltaic cells? Efficient $CsPbBr_3$ cells. J Phys Chem Lett, 2015, 6, 2452
[131] Wang P, Zhang X, Zhou Y, et al. Solvent-controlled growth of inorganic perovskite films in dry environment for efficient and stable solar cells. Nat Commun, 2018, 9, 2225
[132] Sanehira E M, Marshall A R, Christians J A, et al. Enhanced mobility $CsPbI_3$ quantum dot arrays for record-efficiency, high-voltage photovoltaic cells. Sci Adv, 2017, 3, eaao4204
[133] Choi H, Jeong J, Kim H B, et al. Cesium-doped methylammonium lead iodide perovskite light absorber for hybrid solar cells. Nano Energy, 2014, 7, 80
[134] Eperon G E, Paterno G M, Sutton R J, et al. Inorganic caesium lead iodide perovskite solar cells. J Mater Chem A, 2015, 3, 19688
[135] Yao J S, Ge J, Han B N, et al. Ce^{3+}-doping to modulate photoluminescence kinetics for efficient $CsPbBr_3$ nanocrystals based light-emitting diodes. J Am Chem Soc, 2018, 140, 3626
[136] Veldhuis S A, Ng Y F, Ahmad R, et al. Crown ethers enable room-temperature synthesis of $CsPbBr_3$ quantum dots for light-emitting diodes. ACS Energy Lett, 2018, 3, 526
[137] Li Y, Lv Y, Guo Z, et al. One-step preparation of long-term stable and flexible $CsPbBr_3$ perovskite quantum dots/ethylene vinyl acetate copolymer composite films for white light-emitting diodes. ACS Appl Mater Inter, 2018, 10, 15888
[138] Song X, Liu X, Yu D, et al. Boosting two-dimensional MoS_2/$CsPbBr_3$ photodetectors via enhanced light absorbance and interfacial carrier separation. ACS Appl Mater Inter, 2018, 10, 2801
[139] Ramasamy P, Lim D H, Kim B, et al. All-inorganic cesium lead halide perovskite nanocrystals for photodetector applications. Chem Commun, 2016, 52, 2067
[140] Bao C, Yang J, Bai S, et al. High performance and stable all-inorganic metal halide perovskite-based photodetectors for optical communication applications. Adv Mater, 2018, 30, 1803422
[141] Chen Q, Wu J, Ou X, et al. All-inorganic perovskite nanocrystal scintillators. Nature, 2018, 561, 88
[142] Yakunin S, Protesescu L, Krieg F, et al. Low-threshold amplified spontaneous emission and lasing from colloidal nanocrystals of caesium lead halide perovskites. Nat Commun, 2015, 6, 8056
[143] Liu Z, Yang J, Du J, et al. Robust subwavelength single-mode perovskite nanocuboid laser. ACS Nano, 2018, 12, 5923
[144] Zhang Q, Su R, Liu X, et al. High-quality whispering-gallery-mode lasing from cesium lead halide perovskite nanoplatelets. Adv Funct Mater, 2016, 26, 6238
[145] Hou J, Cao S, Wu Y, et al. Inorganic colloidal perovskite quantum dots for robust solar CO_2 reduction. Chem-Eur J, 2017, 23, 9481
[146] Zhou L, Xu Y F, Chen B X, et al. Synthesis and photocatalytic application of stable lead-free $Cs_2AgBiBr_6$ perovskite nanocrystals. Small, 2018, 14, 1703762
[147] Song J, Fang T, Li J, et al. Organic-inorganic hybrid passivation enables perovskite QLEDs with an EQE of 16.48%. Adv Mater, 2018, 30, 1805409
[148] Lin K, Xing J, Quan L N, et al. Perovskite light-emitting diodes with external quantum efficiency exceeding 20 percent. Nature, 2018, 562, 245
[149] Song J, Xu L, Li J, et al. Monolayer and few-layer all-inorganic perovskites as a new family of two-dimensional semiconductors for printable optoelectronic devices. Adv Mater, 2016, 28, 4861
[150] Christians J A, Schulz P, Tinkham J S, et al. Tailored interfaces of unencapsulated perovskite solar cells for > 1000 hour operational stability. Nat Energy, 2018, 3, 68
[151] Sutton R J, Eperon G E, Miranda L, et al. Bandgap-tunable cesium lead halide perovskites with high thermal stability for efficient solar cells. Adv Energy Mater, 2016, 6, 1502458
[152] Swarnkar A, Marshall A R, Sanehira E M, et al. Quantum dot-induced phase stabilization of α-$CsPbI_3$ perovskite for high-efficiency photovoltaics. Science, 2016, 354, 92
[153] Yang S, Chen S, Mosconi E, et al. Stabilizing halide perovskite surfaces for solar cell operation with wide-bandgap lead oxysalts. Science, 2019, 365, 473
[154] Bian H, Bai D, Jin Z, et al. Graded bandgap $CsPbI_{2+x}Br_{1-x}$ perovskite solar cells with a stabilized efficiency of 14.4%. Joule, 2018, 2, 1500
[155] Wang Y, Dar M I, Ono L K, et al. Thermodynamically stabilized β-$CsPbI_3$-based perovskite solar cells with efficiencies > 18%. Science, 2019, 365, 591
[156] Zhang X, Lin H, Huang H, et al. Enhancing the brightness of cesium lead halide perovskite nanocrystal based green light-emitting devices through the interface engineering with perfluorinated ionomer. Nano Lett, 2016, 16, 1415
[157] Song J, Li J, Li X, et al. Quantum dot light-emitting diodes based on inorganic perovskite cesium lead halides ($CsPbX_3$). Adv Mater, 2015, 27, 7162
[158] Yettapu G R, Talukdar D, Sarkar S, et al. Terahertz conductivity within colloidal $CsPbBr_3$ perovskite nanocrystals: remarkably high carrier mobilities and large diffusion lengths. Nano Lett, 2016, 16, 4838
[159] Li F, Ma C, Wang H, et al. Ambipolar solution-processed hybrid perovskite phototransistors. Nat Commun, 2015, 6, 8238

[160] Huo C, Liu X, Wang Z, et al. High-performance low-voltage-driven phototransistors through $CsPbBr_3$-2D crystal van der Waals heterojunctions. Adv Opt Mater, 2018, 6, 1800152

[161] Senanayak S P, Yang B, Thomas T H, et al. Understanding charge transport in lead iodide perovskite thin-film field-effect transistors. Sci Adv, 2017, 3, e1601935

[162] Liu X, Yu D, Song X, et al. Metal halide perovskites: synthesis, ion migration, and application in field-effect transistors. Small, 2018, 14, 1801460

[163] Jellicoe T C, Richter J M, Glass H F J, et al. Synthesis and optical properties of lead-free cesium tin halide perovskite nanocrystals. J Am Chem Soc, 2016, 138, 2941

[164] Leng M, Chen Z, Yang Y, et al. Lead-free, blue emitting bismuth halide perovskite quantum dots. Angew Chem Int Ed, 2016, 55, 15012

[165] Reiss P, Protiere M, Li L. Core/shell semiconductor nanocrystals. Small, 2009, 5, 154